Electronic Research Archive

https://www.aimspress.com/journal/era

ERA, 35(1): 69–99.
DOI: 10.3934/era.2027003
Received: 19 September 2026
Revised: 29 October 2026
Accepted: 02 November 2026
Published: 27 November 2026

Research article

Identifying the initial velocity for a time-fractional diffusion–wave equation from measurements at a single interior point

Ying Chen and Jun Xian*

School of Mathematics and Statistics, Qinghai Normal University, Xining 810008, China

* **Correspondence:** Email: xj_xianjun@163.com.

Abstract: This paper concerns the recovery of the initial velocity in a time-fractional diffusion–wave equation from time-dependent measurements at a single interior point. To address the inherent ill-posedness of the inverse initial-velocity problem, we introduce a Gaussian-type spectral filtering regularization scheme based on the singular system of the forward operator and establish rigorous convergence error bounds. Both a priori and Morozov-type a posteriori parameter-choice rules are analyzed. Finally, one-dimensional and two-dimensional numerical examples are presented to illustrate the reconstruction accuracy and noise stability of the proposed method.

Keywords: time-fractional diffusion–wave equation; inverse initial velocity problem; Gaussian-type spectral filtering regularization; convergence analysis; numerical examples

1. Introduction

Over recent decades, models based on fractional calculus have proven highly effective in capturing anomalous diffusion behaviors, which are fundamentally driven by spatial non-locality and historical memory [1–3]. Specifically, models based on time-fractional diffusion are frequently applied to characterize subdiffusive phenomena within strongly heterogeneous aquifers, porous media, or biological tissues. Meanwhile, the fractional-in-time diffusion–wave framework serves as a fundamental mathematical tool to characterize mechanical wave propagation within viscoelastic media, alongside superdiffusive behaviors found in polymer mixtures and plasmas. Although forward formulations of such models are well-understood, practical engineering scenarios often lack complete knowledge of initial states, boundary conditions, or system parameters, restricting data acquisition to specific discrete locations or time steps. Such problems of determining unknown quantities from additional measurement data are generally referred to as inverse problems. Inverse problems usually face severe mathematical challenges: Although a theoretical solution might exist, it lacks continuous dependence on the input data; consequently, even negligible data perturbations can trigger

catastrophic deviations in the computed result [4, 5]. Therefore, regularization methods are needed to handle such problems.

Over the past few years, inverse problems associated with time-fractional diffusion-wave models have gained substantial attention within the mathematical community, leading to numerous notable contributions. For instance, terminal-time data reconstruction for such equations was examined by Wei and Zhang [6], who established that uniqueness cannot be guaranteed for arbitrary final observation times. In [7], Floridia and Yamamoto further improved the theoretical results concerning the stability and uniqueness of the inverse initial value problem, obtaining conditions on the final time T that ensure the stability of the problem. Shi et al. [8] recovered the initial state through the application of an iterative, generalized, quasi-boundary value regularization technique; Wen and Wang [9] reconstructed the initial value using the quasi-reversibility regularization method; Yang et al. [10] reconstructed the initial value via the Landweber iteration method. Wei and Liao [11] addressed the inverse problem of determining a zeroth-order coefficient dependent on time, providing theoretical guarantees for its uniqueness alongside conditional stability, and reconstructed the coefficient using the Levenberg–Marquardt method. Wei and Xian [12] considered the same problem with integral data, solved the inverse problem numerically using a two-point gradient method, and provided a convergence analysis of the algorithm. Kian et al. [13] investigated a multicoefficient identification problem in higher-dimensional cases; Shi and Cheng [14] studied an inverse Robin coefficient problem; Durdiev and Turdiev [15] demonstrated both the local existence and global uniqueness of the proposed inverse problem by leveraging the contraction mapping principle, successfully determining a time-dependent potential parameter based on integral measurements; Bazhlekova [16] investigated the uniqueness of the solution for an inverse coefficient problem of the multiterm, time-fractional diffusion–wave equation; Wei and Deng [17] recovered the time-dependent potential coefficient using the Tikhonov regularization method; Jing and Yamamoto [18] explored whether multiple parameters—namely the fractional order, the spatial potential, the initial data, and the Robin coefficient—can be uniquely determined in a one-dimensional fractional diffusion–wave model relying solely on point observations at the boundary; Luo et al. [19] reconstructed the space-dependent potential coefficient using an adaptive fractional physics-informed neural networks (fPINNs) method. In [20, 21], Yamamoto established uniqueness for the simultaneous recovery of the fractional order and initial data and for the inverse source problem, respectively, using different types of additional observations.

This study primarily focuses on the inverse initial velocity problem associated with the time-fractional diffusion–wave model. In particular, our research is formulated around the following governing equation:

$$\begin{cases} \partial_{0+}^{\alpha} u(x,t) = \Delta u(x,t) + F(x,t), & x \in \Omega,\ t \in (0,T), \\ u(x,t) = 0, & x \in \partial\Omega,\ t \in (0,T), \\ u(x,0) = a(x), & x \in \Omega, \\ \partial_t u(x,0) = b(x), & x \in \Omega, \end{cases} \tag{1.1}$$

where $\Omega \subset \mathbb{R}^d$ is the spatial domain, and $d \in \{1, 2\}$. We take $\Omega = (0, l)$ with $l > 0$ for $d = 1$ and $\Omega = (0, l_1) \times (0, l_2)$ with $l_1, l_2 > 0$ for $d = 2$. Here, $\partial_{0+}^{\alpha} u$ stands for the Caputo fractional derivative of

order α with respect to time t, defined by

$$\partial_{0+}^{\alpha} u(x,t) = \frac{1}{\Gamma(2-\alpha)} \int_0^t \frac{\partial^2 u(x,s)}{\partial s^2} \frac{ds}{(t-s)^{\alpha-1}}, \quad t > 0, \quad 1 < \alpha < 2, \tag{1.2}$$

where $\Gamma(\cdot)$ denotes the gamma function.

When α, $a(x)$, $b(x)$, and $F(x,t)$ are given, Problem (1.1) is the direct problem for the time-fractional diffusion–wave equation. Its solution theory, well-posedness, and numerical approximation have been extensively studied; see, for example, [22–28].

For $1 < \alpha < 2$, the time-fractional diffusion–wave equation provides an intermediate description between purely diffusive and classical wavelike dynamics. In contrast to the subdiffusion case, two initial data are required: $u(x,0) = a(x)$ and $\partial_t u(x,0) = b(x)$. In wave and viscoelastic interpretations, $a(x)$ represents the initial displacement or initial state, whereas $b(x)$ represents the initial velocity field, the initial rate of temporal change. In practical experiments, the initial velocity may be difficult to measure directly because the excitation occurs before or at the beginning of data acquisition, whereas subsequent temporal responses can often be recorded by a limited number of embedded sensors. This motivates the recovery of $b(x)$ from time-dependent measurements collected at a single accessible interior location.

The present work addresses the inverse problem of using additional data measured at an interior point $x_0 \in \Omega$, namely

$$u(x_0,t) = h(t), \quad t \in (0,T), \tag{1.3}$$

to recover the initial velocity $b(x)$ for $x \in \Omega$.

We focus on two questions: first, whether the initial velocity can be uniquely recovered from the additional data $u(x_0,t) = h(t)$; and second, whether a stable and efficient computational scheme can be devised for the numerical inversion. In practical measurements, interior-point observation data inevitably contain errors. We represent the noisy observation by $h^\delta(t)$ and assume that

$$\|h - h^\delta\|_{L^2(0,T)} \le \delta, \tag{1.4}$$

where $\delta > 0$ is the noise level.

Because the inverse problem is ill-posed, the reconstructed initial velocity does not depend continuously on the observation data; even small perturbations may therefore be strongly amplified. To obtain stable numerical reconstructions, regularization is required. In this study, we employ a Gaussian-type spectral filtering regularization method.

2. Preliminaries

We first collect the spectral notation and auxiliary results used in the subsequent analysis.

Let $\{\lambda_n, \phi_n(x)\}_{n=1}^{\infty}$ be the system of eigenpairs of the operator $-\Delta$ subject to homogeneous Dirichlet boundary conditions

$$\begin{cases} -\Delta\phi_n(x) = \lambda_n \phi_n(x), & x \in \Omega, \\ \phi_n(x) = 0, & x \in \partial\Omega. \end{cases}$$

For $\Omega = (0,l)$, a direct computation yields

$$\lambda_n = \left(\frac{n\pi}{l}\right)^2, \quad \phi_n(x) = \sqrt{\frac{2}{l}} \sin\left(\frac{n\pi x}{l}\right), \quad n = 1,2,3,\ldots$$

For $\Omega = (0, l_1) \times (0, l_2)$, a direct computation yields

$$\lambda_{m,n} = \left(\frac{m\pi}{l_1}\right)^2 + \left(\frac{n\pi}{l_2}\right)^2, \qquad \phi_{m,n}(x^1, x^2) = \sqrt{\frac{2}{l_1}} \sin\frac{m\pi x^1}{l_1} \sqrt{\frac{2}{l_2}} \sin\frac{n\pi x^2}{l_2}, \quad m, n \in \mathbb{N}^+.$$

Because $-\Delta$ is a symmetric uniformly elliptic operator, the corresponding eigenfunctions $\{\phi_n(x)\}_{n=1}^{\infty}$ form an orthonormal basis of $L^2(\Omega)$. Furthermore, we introduce the Hilbert scale space $D((-\Delta)^\gamma)$ $(\gamma \geq 0)$ [22]

$$D((-\Delta)^\gamma) = \left\{ \varphi \in L^2(\Omega) : \sum_{n=1}^{\infty} \lambda_n^{2\gamma} \left|(\varphi, \phi_n)\right|^2 < \infty \right\},$$

and its norm is given by

$$\|\varphi\|_{D((-\Delta)^\gamma)} = \left(\sum_{n=1}^{\infty} \lambda_n^{2\gamma} \left|(\varphi, \phi_n)\right|^2 \right)^{\frac{1}{2}},$$

where $(\cdot, \cdot)$ represents the inner product in $L^2(\Omega)$.

Definition 2.1 ([29])**.** The Mittag-Leffler function is

$$E_{\alpha,\beta}(z) = \sum_{k=0}^{\infty} \frac{z^k}{\Gamma(\alpha k + \beta)}, \qquad z \in \mathbb{C}, \tag{2.1}$$

where $\alpha > 0$ and $\beta \in \mathbb{C}$ are arbitrary constants.

Lemma 2.2 ([17])**.** Let $1 < \alpha < 2$. Assume that

$$a \in D((-\Delta)^{1/\alpha}), \qquad b \in L^2(\Omega), \qquad F \in L^2(0, T; D((-\Delta)^{1/\alpha})).$$

Then, Problem (1.1) admits a unique solution,

$$u \in C\Big([0, T]; D((-\Delta)^{1/\alpha})\Big).$$

Moreover, the solution is represented by

$$\begin{aligned} u(x,t) = &\sum_{n=1}^{\infty} [(a, \phi_n) E_{\alpha,1}(-\lambda_n t^\alpha) + (b, \phi_n) t E_{\alpha,2}(-\lambda_n t^\alpha)] \phi_n(x) \\ &+ \sum_{n=1}^{\infty} \Big(\int_0^t (F(\cdot, \tau), \phi_n)(t-\tau)^{\alpha-1} E_{\alpha,\alpha}\big(-\lambda_n (t-\tau)^\alpha\big)\, d\tau \Big) \phi_n(x). \end{aligned} \tag{2.2}$$

Lemma 2.3 ([30])**.** Let $0 < \alpha < 2$ and $\beta \in \mathbb{R}$ be arbitrary. Assume that ϑ satisfies $\pi\alpha/2 < \vartheta < \min\{\pi, \pi\alpha\}$. Then, there exists a constant $C = C(\alpha, \beta, \vartheta) > 0$ such that

$$\left|E_{\alpha,\beta}(z)\right| \leq \frac{C}{1 + |z|}, \qquad \vartheta \leq |\arg(z)| \leq \pi. \tag{2.3}$$

Definition 2.4 ([31])**.** The Gaussian kernel is defined by

$$V_\mu(t) := \frac{1}{\mu\sqrt{\pi}} \exp\left(-\frac{t^2}{\mu^2}\right), \tag{2.4}$$

where $\mu > 0$ denotes the mollification radius of the averaging filter or the regularization parameter. Moreover, the kernel satisfies

$$\int_{-\infty}^{+\infty} V_\mu(t)dt = 1, \quad \mu > 0.$$

The following uniqueness result is obtained by applying the point-observation uniqueness argument of [20] to the explicit Dirichlet spectral setting considered here.

Corollary 2.5. Let $1 < \alpha < 2$, $a \in D((-\Delta)^{1/\alpha})$, $b_1, b_2 \in L^2(\Omega)$, and $F \in L^2(0,T; D((-\Delta)^{1/\alpha}))$. Let $u_1(x,t) = u(x,t;b_1)$ and $u_2(x,t) = u(x,t;b_2)$ be the solutions of (1.1) with initial velocities b_1 and b_2, respectively, and with the same initial displacement a and source term F. Assume that one of the following two cases holds:

(i) $\Omega = (0,l)$, and $x_0 \in (0,l)$ satisfies $x_0/l \notin \mathbb{Q}$;
(ii) $\Omega = (0,l_1) \times (0,l_2)$, and

$$\frac{l_1^2}{l_2^2} \notin \mathbb{Q}, \qquad x_0 = (x_0^1, x_0^2) \in \Omega, \qquad \frac{x_0^1}{l_1} \notin \mathbb{Q}, \qquad \frac{x_0^2}{l_2} \notin \mathbb{Q}.$$

If $u_1(x_0,t) = u_2(x_0,t)$ for all $t \in (0,T)$, then $b_1 = b_2$ almost everywhere in Ω.

Proof. Set

$$b(x) := b_1(x) - b_2(x), \qquad w(x,t) := u_1(x,t) - u_2(x,t), \quad x \in \Omega, \quad t \in (0,T).$$

Because u_1 and u_2 have the same initial displacement a and the same source term F, the function w satisfies the homogeneous problem

$$\begin{cases} \partial_{0+}^\alpha w(x,t) = \Delta w(x,t), & x \in \Omega, \quad 0 < t < T, \\ w(x,t) = 0, & x \in \partial\Omega, \quad 0 < t < T, \\ w(x,0) = 0, & x \in \Omega, \\ \partial_t w(x,0) = b(x), & x \in \Omega. \end{cases}$$

Accordingly, its spectral representation is

$$w(x,t) = \sum_{n=1}^{\infty} (b, \phi_n)\, tE_{\alpha,2}(-\lambda_n t^\alpha)\phi_n(x),$$

where, in the rectangular case, a single index denotes a fixed enumeration of the two-dimensional modes. The equality $u_1(x_0,t) = u_2(x_0,t)$ therefore gives

$$w(x_0,t) = 0, \qquad 0 < t < T.$$

It remains to verify the spectral nondegeneracy and observation-point conditions used in the point-observation uniqueness argument in [20]. For $\Omega = (0,l)$, the eigenvalues $\lambda_n = (n\pi/l)^2$ are simple. Moreover, if $\phi_n(x_0) = 0$, then $\sin(n\pi x_0/l) = 0$, so $nx_0/l \in \mathbb{Z}$, which would imply $x_0/l \in \mathbb{Q}$, contradicting Assumption (i). Hence, $\phi_n(x_0) \neq 0$ for every $n \geq 1$.

For $\Omega = (0, l_1) \times (0, l_2)$, suppose that $\lambda_{m,n} = \lambda_{p,q}$. Then,

$$m^2 - p^2 = \frac{l_1^2}{l_2^2}(q^2 - n^2).$$

Because $m^2 - p^2$ and $q^2 - n^2$ are integers, whereas $l_1^2/l_2^2 \notin \mathbb{Q}$, the above equality is possible only when $q^2 - n^2 = 0$. Thus, $q = n$, and consequently, $p = m$. Hence, all eigenvalues are simple. Furthermore,

$$\phi_{m,n}(x_0) = \frac{2}{\sqrt{l_1 l_2}} \sin\left(\frac{m\pi x_0^1}{l_1}\right) \sin\left(\frac{n\pi x_0^2}{l_2}\right).$$

The assumptions $x_0^1/l_1 \notin \mathbb{Q}$ and $x_0^2/l_2 \notin \mathbb{Q}$ imply that neither sine factor can vanish for any $m, n \geq 1$; hence, $\phi_{m,n}(x_0) \neq 0$ for every two-dimensional mode.

Therefore, in both cases, the Dirichlet spectrum is simple, and no eigenfunction vanishes at the observation point x_0. These are the spectral nondegeneracy properties required in the point-observation uniqueness argument of [20]. Applying the same argument to the homogeneous problem satisfied by w and using $w(x_0, t) = 0$ on $(0, T)$, we obtain $b = 0$ in $L^2(\Omega)$. Hence, $b_1 = b_2$ almost everywhere in Ω. □

3. Gaussian-type spectral filtering regularization and convergence analysis

We introduce a Gaussian-type spectral filtering strategy to obtain stable approximations of the unknown initial velocity $b(x)$ and establish convergence estimates for both exact and noisy data.

Throughout Sections 3–5, we impose the geometric assumptions on the domain Ω and the interior observation point x_0 stated in Corollary 2.5. In one dimension, $\Omega = (0, l)$ with $l > 0$, and $x_0 \in (0, l)$ satisfies $x_0/l \notin \mathbb{Q}$. In two dimensions, $\Omega = (0, l_1) \times (0, l_2)$ with $l_1, l_2 > 0$ and $l_1^2/l_2^2 \notin \mathbb{Q}$, and $x_0 = (x_0^1, x_0^2) \in \Omega$ satisfies $x_0^1/l_1 \notin \mathbb{Q}$ and $x_0^2/l_2 \notin \mathbb{Q}$. Additional source, noise, and parameter-choice conditions are stated separately where needed. In the rectangular case, a single subscript on an eigenpair denotes a fixed enumeration of the two-dimensional modes.

Throughout this section, we retain the assumptions of Lemma 2.2, namely $a \in D((-\Delta)^{1/\alpha})$, $b \in L^2(\Omega)$, and $F \in L^2(0, T; D((-\Delta)^{1/\alpha}))$. By Lemma 2.2 and the regularity result of [17], we know that $u \in C([0, T]; D((-\Delta)^{1/\alpha}))$. Because $d \in \{1, 2\}$, and $1 < \alpha < 2$, we have $1/\alpha > d/4$; hence, one can choose $\varepsilon_0 > 0$ such that $d/4 + \varepsilon_0 < 1/\alpha$. Therefore, $D((-\Delta)^{1/\alpha}) \hookrightarrow D((-\Delta)^{d/4+\varepsilon_0}) \hookrightarrow H^{d/2+2\varepsilon_0}(\Omega) \hookrightarrow C(\overline{\Omega})$. By the point-observation regularity argument of [17], it follows that $u \in C([0, T]; C(\overline{\Omega}))$, and consequently, $u(x_0, \cdot) \in C([0, T]) \subset L^2(0, T)$.

Because the solution of Eq (1.1) is

$$\begin{aligned} u(x,t) = &\sum_{n=1}^{\infty} \left[(a, \phi_n) E_{\alpha,1}(-\lambda_n t^\alpha) + (b, \phi_n) t E_{\alpha,2}(-\lambda_n t^\alpha)\right] \phi_n(x) \\ &+ \sum_{n=1}^{\infty} \left(\int_0^t (F(\cdot, \tau), \phi_n)(t-\tau)^{\alpha-1} E_{\alpha,\alpha}(-\lambda_n (t-\tau)^\alpha) d\tau \right) \phi_n(x), \end{aligned}$$

at the observation point x_0, introduce the two known functions

$$h^a(t) := \sum_{n=1}^{\infty} (a, \phi_n) E_{\alpha,1}(-\lambda_n t^\alpha) \phi_n(x_0),$$

$$h^f(t) := \sum_{n=1}^{\infty} \left(\int_0^t (F(\cdot,\tau),\phi_n)(t-\tau)^{\alpha-1} E_{\alpha,\alpha}(-\lambda_n (t-\tau)^\alpha)\, d\tau \right) \phi_n(x_0),$$

and set

$$h^{a,f}(t) := h^a(t) + h^f(t).$$

Because $u(x_0,t) = h(t)$, let

$$\tilde{h}(t) := h(t) - h^{a,f}(t) = \sum_{n=1}^{\infty} (b,\phi_n) t E_{\alpha,2}(-\lambda_n t^\alpha)\phi_n(x_0), \quad t \in (0,T). \tag{3.1}$$

For the noisy observation h^δ, define analogously

$$\widetilde{h^\delta}(t) := h^\delta(t) - h^{a,f}(t).$$

To justify the kernel representation, put

$$\alpha_n(t) := t E_{\alpha,2}(-\lambda_n t^\alpha)\phi_n(x_0), \qquad k_J(t,\xi) := \sum_{n=1}^{J} \alpha_n(t)\phi_n(\xi), \quad J \in \mathbb{N}.$$

In two dimensions, the single index denotes a fixed enumeration of the spatial modes. On either of the domains considered above, the eigenfunctions satisfy $|\phi_n(x_0)| \le C_\Omega$, where

$$C_\Omega = \begin{cases} \sqrt{2/l}, & \Omega = (0,l), \\ 2/\sqrt{l_1 l_2}, & \Omega = (0,l_1)\times(0,l_2). \end{cases}$$

Hence, Lemma 2.3 gives

$$\|\alpha_n\|^2_{L^2(0,T)} \le C \int_0^T \frac{t^2}{(1+\lambda_n t^\alpha)^2}\, dt =: C I_n.$$

Set $t_n := \min\{T, \lambda_n^{-1/\alpha}\}$. For all sufficiently large n, $t_n = \lambda_n^{-1/\alpha} < T$, and therefore,

$$\begin{aligned} I_n &\le \int_0^{t_n} t^2\, dt + \lambda_n^{-2} \int_{t_n}^T t^{2-2\alpha}\, dt \\ &\le \begin{cases} C\lambda_n^{-2}, & 1 < \alpha < \dfrac{3}{2}, \\ C\lambda_n^{-2}(1+\log\lambda_n), & \alpha = \dfrac{3}{2}, \\ C\lambda_n^{-3/\alpha}, & \dfrac{3}{2} < \alpha < 2. \end{cases} \end{aligned}$$

In one dimension, $\lambda_n = (n\pi/l)^2$, so each tail is summable. In two dimensions, write $\nu = (m,n) \in \mathbb{N}_+^2$ and $\lambda_\nu = (m\pi/l_1)^2 + (n\pi/l_2)^2$. With $c_0 = \pi^2 \min\{l_1^{-2}, l_2^{-2}\}$, we have $\lambda_\nu \ge c_0(m^2+n^2)$. Grouping the indices by $\max\{m,n\} = q$ gives for every $s > 1$,

$$\sum_{m,n\ge 1} \lambda_{(m,n)}^{-s} \le c_0^{-s} \sum_{q\ge 1} (2q-1) q^{-2s} \le 2c_0^{-s} \sum_{q\ge 1} q^{1-2s} < \infty.$$

The exponents 2 and $3/\alpha$ occurring above are greater than 1. For $\alpha = 3/2$, the logarithmic factor is absorbed using $\lambda^{-2}(1 + \log \lambda) \le C_\varepsilon \lambda^{-2+\varepsilon}$ for sufficiently large λ and any $0 < \varepsilon < 1$. Adding the finitely many remaining terms, we obtain in either case $\sum_{n=1}^{\infty} \|\alpha_n\|^2_{L^2(0,T)} < \infty$.

For $J > L$, spatial orthonormality yields

$$\|k_J - k_L\|^2_{L^2((0,T)\times\Omega)} = \sum_{n=L+1}^{J} \|\alpha_n\|^2_{L^2(0,T)}.$$

Thus, k_J converges in $L^2((0,T)\times\Omega)$ to a kernel k, and

$$\|k\|^2_{L^2((0,T)\times\Omega)} = \sum_{n=1}^{\infty} \|\alpha_n\|^2_{L^2(0,T)} < \infty.$$

Define $B : L^2(\Omega) \to L^2(0,T)$ by this kernel. Then, (3.1) takes the Fredholm form

$$\widetilde{h}(t) = (Bb)(t) = \int_\Omega b(\xi)k(t,\xi)\,d\xi \qquad \text{for a.e. } t \in (0,T). \tag{3.2}$$

Indeed, for every $b \in L^2(\Omega)$, the integral operators with kernels k_J converge to B in operator norm, and their values are the partial sums $\sum_{n=1}^{J}(b,\phi_n)\alpha_n$. In particular, for each fixed m and $J \ge m$, $\int_\Omega k_J(t,\xi)\phi_m(\xi)\,d\xi = \alpha_m(t)$. Passing to the limit in $L^2(0,T)$ gives

$$B\phi_m = \alpha_m. \tag{3.3}$$

Consequently,

$$\sum_{n=1}^{\infty} \|B\phi_n\|^2_{L^2(0,T)} = \|k\|^2_{L^2((0,T)\times\Omega)} < \infty.$$

Hence, B is a Hilbert–Schmidt integral operator and is bounded and compact. Under the standing geometric assumptions, Corollary 2.5 also implies $\mathcal{N}(B) = \{0\}$. Indeed, let $b \in L^2(\Omega)$ satisfy $Bb = 0$ in $L^2(0,T)$. For the corresponding homogeneous problem with $a = 0$ and $F = 0$, the point-observation regularity established above shows that Bb has a continuous representative on $[0,T]$. Because this representative vanishes almost everywhere on $(0,T)$, it vanishes identically there. Corollary 2.5 then yields $b = 0$.

Let $B^* : L^2(0,T) \to L^2(\Omega)$ be the adjoint operator. Let $\{\sigma_n, u_n(\xi), v_n(t)\}$ denote the singular system associated with all nonzero singular values of B:

$$Bu_n = \sigma_n v_n, \qquad B^* v_n = \sigma_n u_n, \qquad \sigma_n > 0. \tag{3.4}$$

The positive singular values are counted with multiplicity and arranged in nonincreasing order. Because B is compact and injective on the infinite-dimensional space $L^2(\Omega)$, it has infinite rank and $\sigma_n \to 0$ as $n \to \infty$. The families $\{u_n\}$ and $\{v_n\}$ form orthonormal bases of $\overline{\mathcal{R}(B^*)} = \mathcal{N}(B)^\perp = L^2(\Omega)$ and $\overline{\mathcal{R}(B)}$, respectively.

Remark. The identity $B\phi_n = \alpha_n$ does not by itself imply $u_n = \phi_n$ or $v_n = \alpha_n/\|\alpha_n\|$. For every n such that $\|\alpha_n\|_{L^2(0,T)} > 0$, we have

$$B^*\left(\frac{\alpha_n}{\|\alpha_n\|_{L^2(0,T)}}\right) = \frac{1}{\|\alpha_n\|_{L^2(0,T)}} \sum_{m=1}^{\infty} (\alpha_m, \alpha_n)_{L^2(0,T)} \phi_m. \tag{3.5}$$

This vector is proportional to ϕ_n only if $(\alpha_m, \alpha_n)_{L^2(0,T)} = 0$ for every $m \neq n$, a property that is not valid in general. Hence, the convergence analysis below must use the true system (3.4). The spatial basis $\{\phi_n\}$ is retained for assembling the forward matrix, whereas its true singular directions are obtained by singular value decomposition (SVD).

The exact initial velocity b is therefore the unique solution of $Bb = \widetilde{h}$. It coincides with the minimum-norm solution, and because $\mathcal{N}(B) = \{0\}$, it automatically satisfies

$$Bb = \widetilde{h}, \qquad b \in \mathcal{N}(B)^{\perp}. \tag{3.6}$$

In the singular system, this unique exact solution satisfies

$$b = \sum_{n=1}^{\infty} (b, u_n) u_n, \qquad \widetilde{h} = \sum_{n=1}^{\infty} \sigma_n (b, u_n) v_n. \tag{3.7}$$

Let $\hat{v}_\mu(\omega)$ be the Fourier transform of the Gaussian kernel $V_\mu(t)$. A direct calculation gives

$$\hat{v}_\mu(\omega) = \exp\left(-\frac{\mu^2 \omega^2}{4}\right). \tag{3.8}$$

Proof. For $\mu > 0$ and $\omega \in \mathbb{R}$, write

$$\widehat{v_\mu}(\omega) = \frac{G_\mu(\omega)}{\mu \sqrt{\pi}}, \qquad G_\mu(\omega) := \int_{\mathbb{R}} e^{-t^2/\mu^2} e^{-i\omega t}\, dt. \tag{3.9}$$

Because $|t| e^{-t^2/\mu^2}$ is integrable, differentiation under the integral sign is justified, and

$$G'_\mu(\omega) = -i \int_{\mathbb{R}} t e^{-t^2/\mu^2} e^{-i\omega t}\, dt = \frac{i\mu^2}{2} \int_{\mathbb{R}} \frac{d}{dt}(e^{-t^2/\mu^2}) e^{-i\omega t}\, dt. \tag{3.10}$$

Integration by parts has a vanishing boundary term and gives

$$G'_\mu(\omega) = -\frac{\mu^2 \omega}{2} G_\mu(\omega). \tag{3.11}$$

Thus, $(d/d\omega)(e^{\mu^2\omega^2/4} G_\mu(\omega)) = 0$. The Gaussian integral gives $G_\mu(0) = \mu \sqrt{\pi}$, and hence,

$$\widehat{v_\mu}(\omega) = \frac{G_\mu(\omega)}{\mu \sqrt{\pi}} = e^{-\mu^2\omega^2/4}. \tag{3.12}$$

□

The mollification method stabilizes ill-posed inverse problems by replacing unstable quantities with appropriately smoothed approximations; Gaussian kernels constitute a classical choice in this context [31–33]. On the other hand, regularization of compact operator equations can be formulated through spectral filter functions acting on the singular system of the forward operator [4, 5]. Motivated by the Gaussian Fourier multiplier [34, 35], we introduce the following Gaussian-type filter on the singular spectrum:

$$\Phi_\mu(\sigma) = \exp\left(-\frac{\mu^2}{4\sigma^2}\right), \quad \sigma > 0. \tag{3.13}$$

It should be emphasized that σ^{-1} is used here as a spectral instability scale and is not identified with the Fourier frequency of the time variable.

Define the regularization operator $R_\mu : L^2(0,T) \to L^2(\Omega)$ by

$$R_\mu z := \sum_{n=1}^{\infty} \exp\left(-\frac{\mu^2}{4\sigma_n^2}\right) \frac{(z, v_n)}{\sigma_n} u_n. \tag{3.14}$$

The regularized solutions corresponding to exact and noisy data are, respectively,

$$b^\mu(x) := R_\mu \widetilde{h} = \sum_{n=1}^{\infty} \exp\left(-\frac{\mu^2}{4\sigma_n^2}\right) \frac{(\widetilde{h}, v_n)}{\sigma_n} u_n(x), \tag{3.15}$$

$$b^{\mu,\delta}(x) := R_\mu \widetilde{h}^\delta = \sum_{n=1}^{\infty} \exp\left(-\frac{\mu^2}{4\sigma_n^2}\right) \frac{(\widetilde{h}^\delta, v_n)}{\sigma_n} u_n(x). \tag{3.16}$$

The corresponding regularized corrected data and regularized observation are denoted, consistently with the original notation, by

$$\widetilde{h}^{\mu,\delta} := B b^{\mu,\delta}, \qquad h^{\mu,\delta} := h^{a,f} + \widetilde{h}^{\mu,\delta}. \tag{3.17}$$

Property 3.1. For every $\mu > 0$, the operator R_μ is bounded and satisfies

$$\left\|R_\mu\right\|_{\mathcal{L}(L^2(0,T),L^2(\Omega))} \le C_2 \mu^{-1}, \qquad C_2 := \sqrt{\frac{2}{\mathrm{e}}}; \tag{3.18}$$

moreover,

$$\left\|I - BR_\mu\right\|_{\mathcal{L}(L^2(0,T))} \le 1. \tag{3.19}$$

For exact data, $b^\mu \to b$ in $L^2(\Omega)$ as $\mu \to 0$. For noisy data, if $\mu = \mu(\delta)$ satisfies

$$\mu(\delta) \to 0, \qquad \frac{\delta}{\mu(\delta)} \to 0 \qquad \text{as } \delta \to 0, \tag{3.20}$$

then $b^{\mu(\delta),\delta} \to b$ in $L^2(\Omega)$.

Proof. For $\sigma > 0$, put $s = \mu/(2\sigma)$. Then,

$$\frac{1}{\sigma} \exp\left(-\frac{\mu^2}{4\sigma^2}\right) = \frac{2}{\mu} s \mathrm{e}^{-s^2}. \tag{3.21}$$

The maximum of $s\mathrm{e}^{-s^2}$ on $(0,\infty)$ is attained at $s = 1/\sqrt{2}$ and equals $1/\sqrt{2\mathrm{e}}$. Thus,

$$\sup_{\sigma>0} \frac{1}{\sigma} \exp\left(-\frac{\mu^2}{4\sigma^2}\right) \le \sqrt{\frac{2}{\mathrm{e}}} \mu^{-1},$$

which proves (3.18). On $\overline{\mathcal{R}(B)}$, the operator BR_μ has eigenvalues $\exp(-\mu^2/(4\sigma_n^2)) \in (0,1)$; it vanishes on $\mathcal{N}(B^*)$. Therefore, (3.19) follows. Using (3.7),

$$b - b^\mu = \sum_{n=1}^{\infty} \left(1 - \exp\left(-\frac{\mu^2}{4\sigma_n^2}\right)\right) (b, u_n) u_n. \tag{3.22}$$

For every fixed n, because the term in parentheses is bounded by 1 and tends to 0 as $\mu \to 0$, an application of Parseval's identity and the Lebesgue dominated convergence theorem yields $\|b - b^\mu\|_{L^2(\Omega)} \to 0$. Furthermore,

$$\begin{aligned}\left\|b^{\mu,\delta} - b\right\|_{L^2(\Omega)} &\le \|b^\mu - b\|_{L^2(\Omega)} + \left\|R_\mu(\widetilde{h}^\delta - \widetilde{h})\right\|_{L^2(\Omega)} \\ &\le \|b^\mu - b\|_{L^2(\Omega)} + C_2\frac{\delta}{\mu};\end{aligned}$$

the parameter conditions (3.20) complete the proof. □

Next, we establish the convergence estimates utilizing an a priori parameter choice strategy.

To derive a convergence rate, we impose a separate operator source condition expressed through the functional calculus of B^*B. Assume that

$$b = (B^*B)^{p/4}w, \qquad \|w\|_{L^2(\Omega)} \le E, \qquad E > 0, \quad 0 < p \le 2; \tag{3.23}$$

equivalently,

$$b = \sum_{n=1}^{\infty} \sigma_n^{p/2}(w, u_n)u_n. \tag{3.24}$$

Theorem 3.2. Assume that the exact solution b satisfies (3.23) and that the noise bound (1.4) holds. For every $\mu > 0$,

$$\left\|b - b^{\mu,\delta}\right\|_{L^2(\Omega)} \le C_1 E\mu^{p/2} + C_2\delta\mu^{-1}, \tag{3.25}$$

where

$$C_1 := 2^{-p/2}\sup_{s>0}\frac{1 - \mathrm{e}^{-s^2}}{s^{p/2}} < \infty, \qquad C_2 := \sqrt{\frac{2}{\mathrm{e}}}. \tag{3.26}$$

If the a priori regularization parameter is chosen as

$$\mu = \left(\frac{\delta}{E}\right)^{\frac{2}{p+2}}, \tag{3.27}$$

then

$$\left\|b - b^{\mu,\delta}\right\|_{L^2(\Omega)} \le C_3 E^{\frac{2}{p+2}}\delta^{\frac{p}{p+2}}, \qquad C_3 := C_1 + C_2. \tag{3.28}$$

Proof. By the triangle inequality

$$\left\|b - b^{\mu,\delta}\right\|_{L^2(\Omega)} \le \|b - b^\mu\|_{L^2(\Omega)} + \left\|b^\mu - b^{\mu,\delta}\right\|_{L^2(\Omega)}, \tag{3.29}$$

we first estimate the approximation error. From (3.15) and (3.24), we have

$$\|b - b^\mu\|^2_{L^2(\Omega)} = \sum_{n=1}^{\infty}\left(1 - \exp\left(-\frac{\mu^2}{4\sigma_n^2}\right)\right)^2 \sigma_n^p\,|(w, u_n)|^2 \tag{3.30}$$

for $s = \mu/(2\sigma)$;

$$\begin{aligned}\left(1 - \exp\left(-\frac{\mu^2}{4\sigma^2}\right)\right)\sigma^{p/2} &= \frac{\mu^{p/2}}{2^{p/2}}\frac{1 - \mathrm{e}^{-s^2}}{s^{p/2}} \\ &\le C_1\mu^{p/2}.\end{aligned} \tag{3.31}$$

The supremum in (3.26) is finite: Near $s = 0$, the quotient is of order $s^{2-p/2}$, and it tends to zero as $s \to \infty$. Therefore,

$$\|b - b^{\mu}\|_{L^2(\Omega)} \le C_1 E \mu^{p/2}. \tag{3.32}$$

For the propagated data error, Property 3.1 gives

$$\begin{aligned} \left\|b^{\mu} - b^{\mu,\delta}\right\|_{L^2(\Omega)} &= \left\|R_{\mu}(\widetilde{h} - \widetilde{h}^{\delta})\right\|_{L^2(\Omega)} \\ &\le C_2 \mu^{-1} \left\|\widetilde{h} - \widetilde{h}^{\delta}\right\|_{L^2(0,T)} \le C_2 \delta \mu^{-1}; \end{aligned} \tag{3.33}$$

combining (3.32) and (3.33) proves (3.25).

To balance the two terms, solve $E\mu^{p/2} = \delta\mu^{-1}$, which gives $\mu^{(p+2)/2} = \delta/E$ and hence (3.27). Substitution into both terms yields

$$E\mu^{p/2} = E^{\frac{2}{p+2}} \delta^{\frac{p}{p+2}}, \qquad \delta\mu^{-1} = E^{\frac{2}{p+2}} \delta^{\frac{p}{p+2}},$$

and (3.28) follows. □

The a priori choice (3.27) is mainly of theoretical value because it requires the source-condition exponent p and the bound E, which are generally unavailable in practical inverse problems. For this reason, the numerical experiments below use the implementable Morozov discrepancy principle rather than the a priori rule.

We next derive convergence estimates for an a posteriori parameter choice.

When the a priori bound E is unavailable, the regularization parameter μ can instead be selected from the noise level by Morozov's discrepancy principle [36, 37].

Define the residual function for $\mu > 0$ by

$$q(\mu) := \left\|Bb^{\mu,\delta} - \widetilde{h}^{\delta}\right\|_{L^2(0,T)}.$$

The Morozov discrepancy principle selects $\mu > 0$ such that

$$q(\mu) = \tau\delta, \tag{3.34}$$

where $\tau > 1$ is fixed.

Lemma 3.3. Suppose that $\mu > 0$ satisfies (3.34). Then,

$$\left\|Bb^{\mu,\delta} - \widetilde{h}\right\|_{L^2(0,T)} \le (\tau + 1)\delta, \tag{3.35}$$

and moreover, if

$$\rho(\mu) := \left\|Bb^{\mu} - \widetilde{h}\right\|_{L^2(0,T)}, \tag{3.36}$$

then

$$(\tau - 1)\delta \le \rho(\mu) \le (\tau + 1)\delta. \tag{3.37}$$

Proof. Applying the triangle inequality yields the first estimate directly:

$$\begin{aligned}\left\|Bb^{\mu,\delta}-\widetilde{h}\right\|_{L^2(0,T)} &\le \left\|Bb^{\mu,\delta}-\widetilde{h}^{\delta}\right\|_{L^2(0,T)}+\left\|\widetilde{h}^{\delta}-\widetilde{h}\right\|_{L^2(0,T)}\\ &\le \tau\delta+\delta=(\tau+1)\delta.\end{aligned}$$

For the second statement, observe that

$$\begin{aligned}Bb^{\mu,\delta}-\widetilde{h}^{\delta}&=(BR_{\mu}-I)\widetilde{h}^{\delta},\\ Bb^{\mu}-\widetilde{h}&=(BR_{\mu}-I)\widetilde{h}.\end{aligned}$$

Using (3.19) and the reverse triangle inequality,

$$\begin{aligned}|q(\mu)-\rho(\mu)| &\le \left\|(I-BR_{\mu})(\widetilde{h}^{\delta}-\widetilde{h})\right\|_{L^2(0,T)}\\ &\le \left\|\widetilde{h}^{\delta}-\widetilde{h}\right\|_{L^2(0,T)}\le\delta.\end{aligned}$$

Because $q(\mu)=\tau\delta$, Ineq (3.37) follows. □

Let P_0 denote the orthogonal projection of $L^2(0,T)$ onto

$$\mathcal{N}(B^*)=\overline{\mathcal{R}(B)}^{\perp}. \tag{3.38}$$

Lemma 3.4. For every $\mu>0$, the residual function q has the spectral representation

$$q(\mu)^2=\left\|P_0\widetilde{h}^{\delta}\right\|^2_{L^2(0,T)}+\sum_{n=1}^{\infty}\left(1-\exp\left(-\frac{\mu^2}{4\sigma_n^2}\right)\right)^2\left|(\widetilde{h}^{\delta},v_n)\right|^2. \tag{3.39}$$

The following conclusions hold:

(i) $q(\mu)$ is continuous and nondecreasing on $(0,\infty)$. It is strictly increasing if the projection of $\widetilde{h}^{\delta}$ onto $\overline{\mathcal{R}(B)}$ is nonzero.

(ii)
$$\lim_{\mu\to 0}q(\mu)=\left\|P_0\widetilde{h}^{\delta}\right\|_{L^2(0,T)}\le\delta. \tag{3.40}$$

(iii)
$$\lim_{\mu\to+\infty}q(\mu)=\left\|\widetilde{h}^{\delta}\right\|_{L^2(0,T)}; \tag{3.41}$$

consequently, if

$$\left\|\widetilde{h}^{\delta}\right\|_{L^2(0,T)}>\tau\delta, \tag{3.42}$$

then there exists a unique $\mu>0$ satisfying (3.34).

Proof. Because $BR_{\mu}v_n=\exp(-\mu^2/(4\sigma_n^2))v_n$, and BR_{μ} vanishes on $\mathcal{N}(B^*)$, the orthogonal decomposition

$$\widetilde{h}^{\delta}=P_0\widetilde{h}^{\delta}+\sum_{n=1}^{\infty}(\widetilde{h}^{\delta},v_n)v_n$$

gives (3.39). Each summand is continuous and nondecreasing in μ. It is bounded by $|(\widetilde{h}^\delta, v_n)|^2$, whose sum is finite. Dominated convergence therefore proves continuity and the two limits. Strict monotonicity follows whenever at least one coefficient $(\widetilde{h}^\delta, v_n)$ is nonzero.

Because the exact data satisfy $\widetilde{h} = Bb \in \mathcal{R}(B)$,

$$\begin{aligned}\left\|P_0\widetilde{h}^\delta\right\|_{L^2(0,T)} &= \left\|P_0(\widetilde{h}^\delta - \widetilde{h})\right\|_{L^2(0,T)} \\ &\le \left\|\widetilde{h}^\delta - \widetilde{h}\right\|_{L^2(0,T)} \le \delta,\end{aligned}$$

which proves (3.40). Under (3.42), the value $\tau\delta$ lies strictly between the limits in (3.40) and (3.41). The intermediate value theorem gives existence. The same strict inequalities guarantee that the range projection is nonzero, and hence, strict monotonicity gives uniqueness. □

Theorem 3.5. Assume that the source condition (3.23), the noise condition (1.4), and the nontriviality condition (3.42) hold. Let $\mu > 0$ be selected by the Morozov discrepancy principle (3.34). Then,

$$\left\|b - b^{\mu,\delta}\right\|_{L^2(\Omega)} \le C_5(\tau, p) E^{\frac{2}{p+2}} \delta^{\frac{p}{p+2}}, \tag{3.43}$$

where

$$C_5(\tau, p) := (\tau + 1)^{\frac{p}{p+2}} + C_2 \left(\frac{D_p}{\tau - 1}\right)^{\frac{2}{p+2}}, \tag{3.44}$$

$$D_p := 2^{-\frac{p+2}{2}} \sup_{s>0} \frac{1 - \mathrm{e}^{-s^2}}{s^{(p+2)/2}} < \infty; \tag{3.45}$$

in particular, $b^{\mu,\delta} \to b$ in $L^2(\Omega)$ as $\delta \to 0$.

Proof. We split the total error as

$$\left\|b - b^{\mu,\delta}\right\|_{L^2(\Omega)} \le \|b - b^\mu\|_{L^2(\Omega)} + \left\|b^\mu - b^{\mu,\delta}\right\|_{L^2(\Omega)}. \tag{3.46}$$

First, set

$$r_n(\mu) := 1 - \exp\left(-\frac{\mu^2}{4\sigma_n^2}\right), \qquad \theta := \frac{p}{p+2}; \tag{3.47}$$

by (3.24),

$$\begin{aligned}\|b - b^\mu\|^2_{L^2(\Omega)} &= \sum_{n=1}^{\infty} r_n(\mu)^2 \sigma_n^p \left|(w, u_n)\right|^2 \\ &= \sum_{n=1}^{\infty} \left[r_n(\mu)^2 \sigma_n^{p+2} \left|(w, u_n)\right|^2\right]^\theta \left[r_n(\mu)^2 \left|(w, u_n)\right|^2\right]^{1-\theta}.\end{aligned}$$

Hölder's inequality with exponents $1/\theta$ and $1/(1-\theta)$ gives

$$\begin{aligned}\|b - b^\mu\|^2_{L^2(\Omega)} &\le \left(\sum_{n=1}^{\infty} r_n(\mu)^2 \sigma_n^{p+2} \left|(w, u_n)\right|^2\right)^\theta \left(\sum_{n=1}^{\infty} r_n(\mu)^2 \left|(w, u_n)\right|^2\right)^{1-\theta} \\ &\le \rho(\mu)^{2\theta} E^{2(1-\theta)}.\end{aligned} \tag{3.48}$$

Taking the square root and applying the upper bound in (3.37), we obtain

$$\|b - b^{\mu}\|_{L^2(\Omega)} \leq (\tau + 1)^{\frac{p}{p+2}} E^{\frac{2}{p+2}} \delta^{\frac{p}{p+2}}. \tag{3.49}$$

It remains to estimate the propagated noise. Again, by the source condition

$$\rho(\mu)^2 = \sum_{n=1}^{\infty} r_n(\mu)^2 \sigma_n^{p+2} |(w, u_n)|^2 \tag{3.50}$$

for $s = \mu/(2\sigma)$,

$$\begin{aligned}\left(1 - \exp\left(-\frac{\mu^2}{4\sigma^2}\right)\right)\sigma^{(p+2)/2} &= \frac{\mu^{(p+2)/2}}{2^{(p+2)/2}} \frac{1 - \mathrm{e}^{-s^2}}{s^{(p+2)/2}} \\ &\leq D_p \mu^{(p+2)/2};\end{aligned}$$

the constant D_p is finite for $0 < p \leq 2$. Near zero, the quotient is of order $s^{(2-p)/2}$, and at infinity, it tends to zero. Hence,

$$\rho(\mu) \leq D_p E \mu^{(p+2)/2}, \tag{3.51}$$

and combining this estimate with the lower bound in (3.37) gives

$$\mu \geq \left(\frac{(\tau - 1)\delta}{D_p E}\right)^{\frac{2}{p+2}}. \tag{3.52}$$

Therefore, by Property 3.1,

$$\left\|b^{\mu} - b^{\mu,\delta}\right\|_{L^2(\Omega)} \leq C_2 \frac{\delta}{\mu} \leq C_2 \left(\frac{D_p}{\tau - 1}\right)^{\frac{2}{p+2}} E^{\frac{2}{p+2}} \delta^{\frac{p}{p+2}}, \tag{3.53}$$

and combining (3.49) and (3.53) proves (3.43). □

It is useful to compare the rate obtained above with classical regularization theory. Writing $\nu = p/4$, the source condition (3.23) takes the standard form $b = (B^*B)^{\nu} w$. For classical Tikhonov regularization, this source condition yields the order $O\left(\delta^{2\nu/(2\nu+1)}\right)$ under an appropriate parameter choice; because $\nu = p/4$, this is exactly $O\left(\delta^{p/(p+2)}\right)$, the same order as (3.28) and (3.43). Discrepancy-stopped Landweber iteration has an analogous order under corresponding source assumptions; see, for example, the general regularization theory in [4,37] and the Landweber-type application in [10]. Thus, the present Gaussian-type spectral filter is comparable in convergence order with these classical methods; its role here is to provide a different spectral damping mechanism together with explicit a priori and Morozov-type error estimates for the present inverse initial-velocity problem.

4. Numerical discretization

We retain the geometric assumptions on Ω and x_0 stated in Section 3. This section discretizes the forward operator by spatial and temporal orthogonal projections and then applies the Gaussian-type spectral filter from Section 3 to the resulting matrix. We describe the one-dimensional and two-dimensional constructions separately. All series expansions below are understood in the corresponding L^2 spaces.

4.1. One-dimensional discretization

For $\Omega = (0, l)$, we use the spatial eigenfunctions $\{\phi_n\}_{n\geq 1}$ and the following orthonormal sine basis of $L^2(0, T)$:

$$\psi_k(t) := \sqrt{\frac{2}{T}} \sin\left(\frac{k\pi t}{T}\right), \qquad k = 1, 2, \ldots. \tag{4.1}$$

Expand $\alpha_n(t)$ and $\widetilde{h}(t)$ in the temporal basis and $b(\xi)$ in the spatial basis:

$$\alpha_n(t) = \sum_{k=1}^{\infty} A_{nk}\psi_k(t), \quad b(\xi) = \sum_{n=1}^{\infty} b_n\phi_n(\xi), \quad \widetilde{h}(t) = \sum_{k=1}^{\infty} H_k\psi_k(t), \tag{4.2}$$

in which

$$A_{nk} := (\alpha_n, \psi_k), \qquad b_n := (b, \phi_n), \qquad H_k := (\widetilde{h}, \psi_k). \tag{4.3}$$

For noisy corrected data, define

$$H_k^{\delta} := (\widetilde{h^{\delta}}, \psi_k) = (h^{\delta}, \psi_k) - H_k^{a,f}, \qquad H_k^{a,f} := (h^{a,f}, \psi_k). \tag{4.4}$$

The coefficients of the continuous regularized corrected data $\widetilde{h}^{\mu,\delta}$ defined in (3.17) are

$$H_k^{\mu,\delta} := (\widetilde{h}^{\mu,\delta}, \psi_k). \tag{4.5}$$

By the boundedness of B, for each fixed k, we have

$$H_k = (Bb, \psi_k) = \lim_{L\to\infty}\left(B\sum_{n=1}^{L} b_n\phi_n, \psi_k\right) = \lim_{L\to\infty}\sum_{n=1}^{L} A_{nk}b_n.$$

The scalar series is absolutely convergent, as

$$\sum_{n=1}^{\infty} |A_{nk}b_n| \leq \|b\|_{L^2(\Omega)}\|B^*\psi_k\|_{L^2(\Omega)} < \infty.$$

Consequently, the infinite coefficient system is

$$\sum_{n=1}^{\infty} A_{nk}b_n = H_k, \qquad k = 1, 2, \ldots. \tag{4.6}$$

Choose positive integers M and N. Let $A_{M,N} \in \mathbb{R}^{M\times N}$ be the matrix whose (k, n)-entry is A_{nk}, and define

$$\boldsymbol{b}_N := (b_1, \ldots, b_N)^{\mathsf{T}}, \qquad \boldsymbol{H}_M^{\delta} := (H_1^{\delta}, \ldots, H_M^{\delta})^{\mathsf{T}}, \tag{4.7}$$

where $\boldsymbol{b}_N$ contains the coefficients of the exact solution. Let Q_N be the spatial orthogonal projection onto the subspace spanned by $\phi_1, \ldots, \phi_N$. With exact matrix entries and data projection coefficients, the truncated data satisfy

$$\boldsymbol{H}_M^{\delta} = A_{M,N}\boldsymbol{b}_N + \boldsymbol{e}_M^{\delta} + \boldsymbol{r}_{M,N}, \tag{4.8}$$

where for $k = 1, \dots, M$,

$$(\boldsymbol{e}_M^\delta)_k = (\widetilde{h}^\delta - \widetilde{h}, \psi_k), \qquad (\boldsymbol{r}_{M,N})_k = (B(I - Q_N)b, \psi_k).$$

Thus, the finite-dimensional inverse problem is represented by

$$A_{M,N}\boldsymbol{c} \approx \boldsymbol{H}_M^\delta, \qquad \boldsymbol{c} \in \mathbb{R}^N,$$

with both the observation noise and spatial truncation error included in the data error bound.

We compute the reduced singular value decomposition

$$A_{M,N} = U_r \Sigma_r V_r^\mathsf{T}, \qquad \Sigma_r = \operatorname{diag}(\sigma_1^{M,N}, \dots, \sigma_r^{M,N}), \qquad \sigma_j^{M,N} > 0, \tag{4.9}$$

where $r = \operatorname{rank}(A_{M,N})$. Denote the columns of U_r and V_r by $\boldsymbol{v}_j$ and $\boldsymbol{u}_j$, respectively, so that the notation agrees with the continuous singular system: $\boldsymbol{u}_j$ is a right-singular vector, and $\boldsymbol{v}_j$ is a left-singular vector.

The discrete Gaussian spectral mollification solution is

$$\begin{aligned} \boldsymbol{b}_N^{\mu,\delta} &:= \sum_{j=1}^r \exp\left(-\frac{\mu^2}{4(\sigma_j^{M,N})^2}\right) \frac{(\boldsymbol{H}_M^\delta, \boldsymbol{v}_j)_{\mathbb{R}^M}}{\sigma_j^{M,N}} \boldsymbol{u}_j \\ &= V_r \operatorname{diag}\left(\frac{\exp(-\mu^2/(4(\sigma_j^{M,N})^2))}{\sigma_j^{M,N}}\right)_{j=1}^r U_r^\mathsf{T} \boldsymbol{H}_M^\delta. \end{aligned} \tag{4.10}$$

The reconstructed initial velocity is

$$b_N^{\mu,\delta}(x) := \sum_{n=1}^N (\boldsymbol{b}_N^{\mu,\delta})_n \phi_n(x). \tag{4.11}$$

Define the corrected data generated by the discrete reconstruction as

$$\widetilde{h}_N^{\mu,\delta} := B b_N^{\mu,\delta}.$$

Its first M temporal coefficients form the vector

$$\boldsymbol{H}_{M,N}^{\mu,\delta} := ((\widetilde{h}_N^{\mu,\delta}, \psi_k))_{k=1}^M = A_{M,N} \boldsymbol{b}_N^{\mu,\delta}, \tag{4.12}$$

where the coefficient tuple is understood as a column vector. In general, $\boldsymbol{H}_{M,N}^{\mu,\delta}$ differs from $(H_1^{\mu,\delta}, \dots, H_M^{\mu,\delta})^\mathsf{T}$ defined by (4.5): Discretizing B before spectral filtering need not give the projection of the continuous regularized data.

The discrete residual is

$$\begin{aligned} q_{M,N}(\mu)^2 :=& \left\| A_{M,N} \boldsymbol{b}_N^{\mu,\delta} - \boldsymbol{H}_M^\delta \right\|_2^2 \\ =& \sum_{j=1}^r \left(1 - \exp\left(-\frac{\mu^2}{4(\sigma_j^{M,N})^2}\right)\right)^2 \left| (\boldsymbol{H}_M^\delta, \boldsymbol{v}_j)_{\mathbb{R}^M} \right|^2 \\ &+ \left\| (I - U_r U_r^\mathsf{T}) \boldsymbol{H}_M^\delta \right\|_2^2. \end{aligned} \tag{4.13}$$

For exact matrix entries and data projection coefficients, let $\eta_{M,N} > 0$ be a known upper bound for the effective discrete data error:

$$\|\boldsymbol{H}_M^\delta - A_{M,N}\boldsymbol{b}_N\|_2 \le \eta_{M,N}.$$

By (4.8) and $\|\boldsymbol{e}_M^\delta\|_2 \le \delta$, a sufficient bound is

$$\eta_{M,N} \ge \delta + \|\boldsymbol{r}_{M,N}\|_2.$$

For $\tau > 1$, Eq (4.13) shows that $q_{M,N}(\mu) = \tau\eta_{M,N}$ has a unique solution $\mu > 0$ whenever

$$\|(I - U_r U_r^\top)\boldsymbol{H}_M^\delta\|_2 < \tau\eta_{M,N} < \|\boldsymbol{H}_M^\delta\|_2.$$

Indeed, these are the limits of $q_{M,N}$ as $\mu \to 0$ and $\mu \to \infty$, and the strict inequalities ensure that at least one coefficient $(\boldsymbol{H}_M^\delta, \boldsymbol{v}_j)_{\mathbb{R}^M}$ is nonzero. Hence, $q_{M,N}$ is continuous and strictly increasing between these limits. Moreover, because $(I - U_r U_r^\top)A_{M,N} = 0$, the effective error bound implies

$$\|(I - U_r U_r^\top)\boldsymbol{H}_M^\delta\|_2 \le \|\boldsymbol{H}_M^\delta - A_{M,N}\boldsymbol{b}_N\|_2 \le \eta_{M,N} < \tau\eta_{M,N}.$$

For numerical assembly, write

$$\widehat{A}_{M,N} = A_{M,N} + \Delta A_{M,N}, \qquad \widehat{\boldsymbol{H}}_M^\delta = \boldsymbol{H}_M^\delta + \Delta\boldsymbol{H}_M,$$

where $\Delta\boldsymbol{H}_M$ includes errors in the temporal data coefficients and the known-data correction. Then, Eq (4.8) gives

$$\widehat{\boldsymbol{H}}_M^\delta - \widehat{A}_{M,N}\boldsymbol{b}_N = \boldsymbol{e}_M^\delta + \boldsymbol{r}_{M,N} + \Delta\boldsymbol{H}_M - \Delta A_{M,N}\boldsymbol{b}_N.$$

Thus, a sufficient bound for the effective error of the assembled system is

$$\eta_{M,N} \ge \delta + \|\boldsymbol{r}_{M,N}\|_2 + \|\Delta\boldsymbol{H}_M\|_2 + \|\Delta A_{M,N}\|_2\|\boldsymbol{b}_N\|_2,$$

where the matrix norm is the induced Euclidean norm. In implementation, solution-dependent quantities in these bounds must be controlled by available a priori bounds or discretization error estimates. When the assembled pair $(\widehat{A}_{M,N}, \widehat{\boldsymbol{H}}_M^\delta)$ is used, its SVD, filtered reconstruction, and residual must all be computed from that pair. The same discrepancy argument applies with $\eta_{M,N}$ bounding $\|\widehat{\boldsymbol{H}}_M^\delta - \widehat{A}_{M,N}\boldsymbol{b}_N\|_2$.

4.2. Two-dimensional discretization

Consider the rectangular domain $\Omega = (0, l_1)\times(0, l_2)$ with an interior observation point $\mathbf{x}_0 = (x_0^1, x_0^2) \in \Omega$. Under homogeneous Dirichlet boundary conditions, the eigenpairs of $-\Delta$ are

$$\lambda_{mn} = \left(\frac{m\pi}{l_1}\right)^2 + \left(\frac{n\pi}{l_2}\right)^2, \qquad \phi_{mn}(x, y) = \sqrt{\frac{2}{l_1}}\sin\left(\frac{m\pi x}{l_1}\right)\sqrt{\frac{2}{l_2}}\sin\left(\frac{n\pi y}{l_2}\right), \quad m, n \in \mathbb{N}^+. \tag{4.14}$$

In this case, Eqs (3.1) and (3.2) become

$$\tilde{h}(t) = (Bb)(t) = \sum_{m,n=1}^{\infty} b_{mn}\alpha_{mn}(t), \qquad \alpha_{mn}(t) = tE_{\alpha,2}(-\lambda_{mn}t^\alpha)\phi_{mn}(\mathbf{x}_0), \tag{4.15}$$

where $b_{mn} = (b, \phi_{mn})$. Let $\{\psi_k\}_{k\geq 1}$ be the time basis in (4.1), and define the following coefficients:

$$A_{k,(mn)} := (\alpha_{mn}, \psi_k), \quad H_k := (\tilde{h}, \psi_k), \quad H_k^{\delta} := (h^{\delta}, \psi_k) - H_k^{a,f}. \tag{4.16}$$

Because B is bounded, taking the inner product of $Bb = \tilde{h}$ with ψ_k yields

$$\sum_{m,n\geq 1} A_{k,(mn)}\, b_{mn} = H_k, \qquad k = 1, 2, \ldots \tag{4.17}$$

Choose positive integers M, N_1, N_2, let $N = N_1 N_2 \leq M$, and define the retained index set

$$\mathcal{J}_N := \{1, \ldots, N_1\} \times \{1, \ldots, N_2\}.$$

We arrange the pairs $(m, n) \in \mathcal{J}_N$ lexicographically:

$$j = (m-1)N_2 + n, \qquad j = 1, \ldots, N, \tag{4.18}$$

and we write $\boldsymbol{b}_N = (b_1, \ldots, b_N)^{\mathrm{T}}$ and $\boldsymbol{H}_M^{\delta} = (H_1^{\delta}, \ldots, H_M^{\delta})^{\mathrm{T}}$, where $b_j = b_{mn}$. Let $A_{M,N} \in \mathbb{R}^{M\times N}$ be the matrix with entries $(A_{M,N})_{k,j} = A_{k,(mn)}$. The truncated system is

$$A_{M,N}\boldsymbol{c} \approx \boldsymbol{H}_M^{\delta}, \ \boldsymbol{c} \in \mathbb{R}^N. \tag{4.19}$$

We compute the reduced singular value decomposition $A_{M,N} = U_r \Sigma_r V_r^{\mathrm{T}}$, $r = \mathrm{rank}(A_{M,N})$ as in (4.9). Let the column vectors of U_r and V_r be denoted by $\boldsymbol{v}_j$ and $\boldsymbol{u}_j$, respectively, and the positive singular values be $\sigma_j^{M,N}$. The discrete Gaussian spectral filtering solution is

$$\boldsymbol{b}_N^{\mu,\delta} = \sum_{j=1}^{r} \exp\left(-\frac{\mu^2}{4(\sigma_j^{M,N})^2}\right) \frac{(\boldsymbol{H}_M^{\delta}, \boldsymbol{v}_j)_{\mathbb{R}^M}}{\sigma_j^{M,N}} \boldsymbol{u}_j. \tag{4.20}$$

If $r = 0$, the above summation is defined to be zero. In particular, continuous injectivity alone does not guarantee full column rank for every finite choice of (M, N). Therefore, the reconstructed initial velocity is

$$b_{N_1,N_2}^{\mu,\delta}(x_1, x_2) = \sum_{m=1}^{N_1} \sum_{n=1}^{N_2} (\boldsymbol{b}_N^{\mu,\delta})_{(m-1)N_2+n} \phi_{m,n}(x_1, x_2). \tag{4.21}$$

By rearranging the coefficients into a matrix $C \in \mathbb{R}^{N_1\times N_2}$ with $C_{m,n} = (\boldsymbol{b}_N^{\mu,\delta})_{(m-1)N_2+n}$, the reconstructed values on the tensor grid $\{x_{1,i}\} \times \{x_{2,j}\}$ can be written as

$$B_{\mathrm{grid}} = \Phi_1 C \Phi_2^{\top},$$

where

$$(\Phi_1)_{i,m} = \sqrt{\frac{2}{l_1}} \sin\left(\frac{m\pi x_{1,i}}{l_1}\right), \quad (\Phi_2)_{j,n} = \sqrt{\frac{2}{l_2}} \sin\left(\frac{n\pi x_{2,j}}{l_2}\right).$$

When the reconstruction error is evaluated on the grid, a quadrature-weighted discrete L^2-norm should be used.

Let $P_M : L^2(0, T) \to \mathrm{span}\{\psi_1, \ldots, \psi_M\}$ be the temporal orthogonal projection. Assume that the matrix entries and temporal data coefficients are computed using exact $L^2(0, T)$ inner products.

Because the time basis is orthonormal, the coefficient residual equals the L^2-norm of the projected residual generated by the reconstructed function in (4.21):

$$q_{M,N}(\mu) = \|A_{M,N}\boldsymbol{b}_N^{\mu,\delta} - \boldsymbol{H}_M^{\delta}\|_2 = \|P_M(Bb_{N_1,N_2}^{\mu,\delta} - \tilde{h}^{\delta})\|_{L^2(0,T)}. \tag{4.22}$$

Hence, $q_{M,N}$ is not an unweighted residual directly computed from the original time-sampled values but rather a residual obtained based on the orthonormal temporal projection coefficients.

Let $P_{\mathcal{J}_N} : L^2(\Omega) \to \mathrm{span}\{\phi_{m,n} : (m,n) \in \mathcal{J}_N\}$ be the spatial orthogonal projection. Under the same exact assembly and projection assumptions, the two-dimensional analog of (4.8) is

$$\boldsymbol{H}_M^{\delta} = A_{M,N}\boldsymbol{b}_N + \boldsymbol{e}_M^{\delta} + \boldsymbol{r}_{M,N}, \tag{4.23}$$

where

$$(\boldsymbol{e}_M^{\delta})_k = (\tilde{h}^{\delta} - \tilde{h}, \psi_k)_{L^2(0,T)}, \qquad (\boldsymbol{r}_{M,N})_k = (B(I - P_{\mathcal{J}_N})b, \psi_k)_{L^2(0,T)}.$$

By the contractivity of orthogonal projections, we obtain

$$\|\boldsymbol{e}_M^{\delta}\|_2 \le \delta$$

and

$$\|\boldsymbol{r}_{M,N}\|_2 = \|P_M B(I - P_{\mathcal{J}_N})b\|_{L^2(0,T)} \le \|B\|_{\mathcal{L}(L^2(\Omega),L^2(0,T))}\|(I - P_{\mathcal{J}_N})b\|_{L^2(\Omega)}.$$

For numerical assembly, the perturbation identity and effective error bounds given above apply with Q_N replaced by $P_{\mathcal{J}_N}$. The SVD, filtered reconstruction, and residual must consistently use the same assembled matrix and data.

Finally, due to the orthogonality between the retained and discarded modes, we obtain the following exact error decomposition:

$$\|b_{N_1,N_2}^{\mu,\delta} - b\|_{L^2(\Omega)}^2 = \|\boldsymbol{b}_N^{\mu,\delta} - \boldsymbol{b}_N\|_2^2 + \sum_{(m,n)\notin\mathcal{J}_N} |b_{m,n}|^2. \tag{4.24}$$

The first term on the right-hand side represents the coefficient recovery error on the retained spatial modes, and the second term is the spatial truncation error. Temporal projection and, in an implementation, numerical quadrature affect the coefficient recovery error and must be controlled together with the observation noise.

We emphasize that the convergence rates in Section 3 are established for the continuous operator B, whereas the computations use the projected matrix $A_{M,N}$. The finite-dimensional method is therefore an approximation of the continuous regularization procedure. Its total error contains, in addition to the regularization and data errors, the spatial truncation, temporal projection, and numerical assembly errors quantified above. Consequently, the continuous rates should not be interpreted as discrete convergence rates without additional assumptions linking M, N, the discretization errors, and the regularization parameter.

5. Numerical examples

To evaluate the efficacy and stability of the proposed Gaussian-type spectral filtering regularization scheme for initial velocity reconstruction, this section presents several numerical examples.

Given that errors are inevitable in practical physical measurements, the noisy data used for testing are generated by

$$h^\delta = h + \epsilon h(2\mathrm{rand}(\cdot) - 1), \tag{5.1}$$

where at each temporal sampling point t_j, independent pseudorandom variables $r_j \sim U(0,1)$ are generated, and $\xi_j = 2r_j - 1 \sim U(-1,1)$ is used in the perturbation $h^\delta(t_j) = h(t_j) + \epsilon h(t_j)\xi_j$. The same random seed is used for all noise levels so that the underlying noise realization is unchanged when ϵ varies. The parameter ϵ controls the amplitude of the multiplicative perturbation, whereas $\delta = \|h^\delta - h\|_{L^2(0,T)}$ denotes the realized continuous-data noise level. In the discrete implementation, temporal inner products are evaluated by the composite trapezoidal rule. In particular,

$$(\boldsymbol{e}_M^\delta)_k \approx \int_0^T (h^\delta - h)\psi_k \, dt, \qquad \delta_M := \|\boldsymbol{e}_M^\delta\|_2,$$

and all discrepancy-principle parameter choices in Section 5 use $\tau = 1.01$. Except for the parameter-sensitivity studies in Tables 5–7, where μ is prescribed or varied deliberately, the Gaussian regularization parameter for nonzero-noise data is determined by the discrete Morozov equation $q_{M,N}(\mu) = \tau\delta_M$; for noise-free data, we use the limiting value $\mu = 0$, corresponding to the reduced pseudoinverse. As noted after Theorem 3.2, the a priori rule (3.27) is not used in the computations because it requires the generally unavailable source parameters p and E.

For the purpose of quantifying inversion accuracy, we use the relative L^2 error

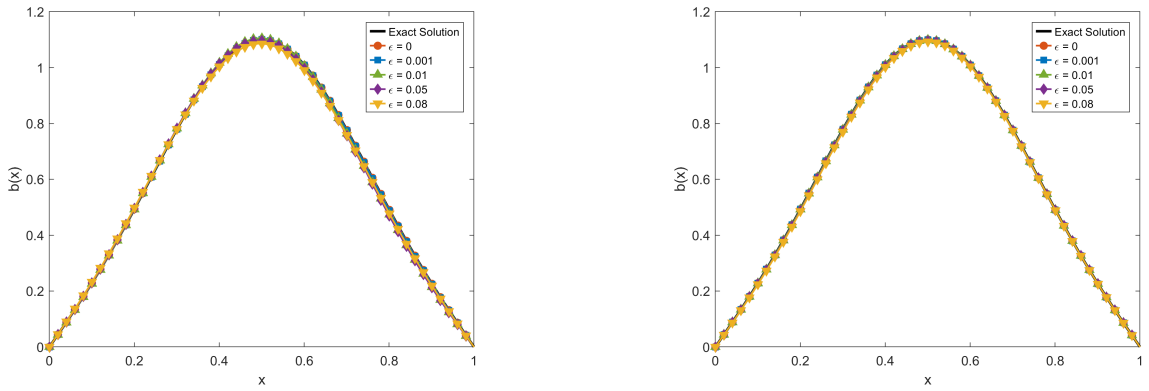
$$e_r(b,\epsilon) = \frac{\|b^{\mu,\delta} - b\|_{L^2(\Omega)}}{\|b\|_{L^2(\Omega)}}. \tag{5.2}$$

The spatial L^2 norms are evaluated by the composite trapezoidal rule in one dimension and by the tensor-product trapezoidal rule in two dimensions.

5.1. One-dimensional case

In the one-dimensional numerical examples, we set the truncation number of the time basis functions to $M = 64$ and the maximum truncation number of the spatial basis functions to $N = 8$. To construct the exact data $h(t) = u(x_0, t)$ at the interior observation point, we first solve the forward problem through mesh partitioning. In the computation, the spatial interval length is fixed at $l = 1$, the terminal observation time at $T = 1$, and the numbers of spatial and temporal grid nodes to $N_x = 1000$ and $N_t = 2000$, respectively. The observation points specified below satisfy $x_0/l \notin \mathbb{Q}$, in accordance with Corollary 2.5 and the standing geometric assumptions in Sections 3 and 4.

Example 1. Let the true initial velocity be $b(x) = \sin(\pi x) - 0.1\sin(3\pi x)$, with $a(x) = 0.5\sin(\pi x) + 0.2\sin(2\pi x)$ and $F(x,t) = (2\sin(\pi x) - \sin(3\pi x))e^{-t}$. The observation point is $x_0 = 0.085 + \sqrt{2}/10{,}000$, and we take $N = 4$. Figure 1 shows the reconstructions for $\alpha = 1.2$ and $\alpha = 1.8$ under different noise levels. Table 1 presents the relative errors along with the values of μ at different noise levels for the two fractional orders.



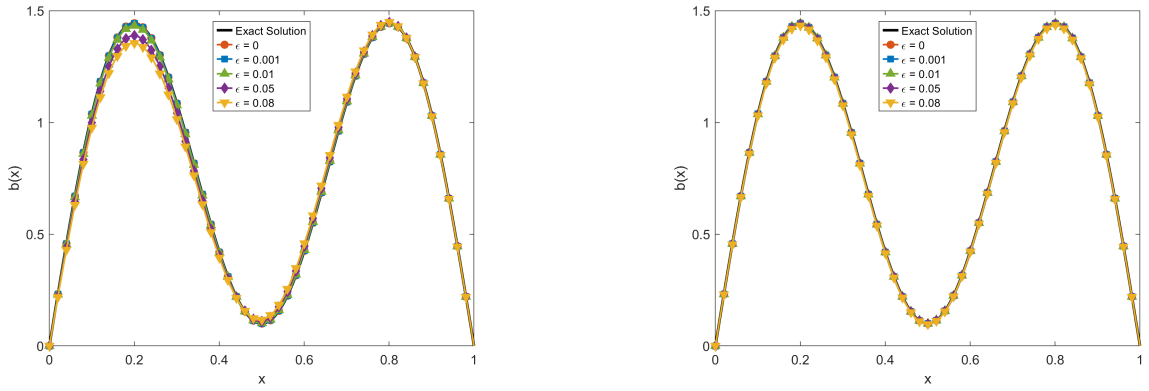
(a) $\alpha = 1.2$ **(b)** $\alpha = 1.8$

Figure 1. Numerical reconstructions for Example 1 under various noise levels with $\alpha = 1.2$ and $\alpha = 1.8$.

Table 1. Relative errors and μ under different noise levels for Example 1.

$e_r(\mu)$ ϵ / α	0	0.001	0.01	0.05	0.08
1.2	1.92e-09 (0)	1.58e-03 (4.30e-04)	1.13e-02 (1.34e-03)	1.60e-02 (2.87e-03)	1.54e-02 (3.56e-03)
1.8	8.34e-11 (0)	1.01e-04 (1.09e-03)	1.01e-03 (3.43e-03)	5.02e-03 (7.68e-03)	8.03e-03 (9.72e-03)

Example 2. Let the true initial velocity be $b(x) = \sin(\pi x) + 0.9\sin(3\pi x)$, with $a(x) = 0.5\sin(2\pi x)$ and $F(x,t) = (0.3\sin(\pi x) + 0.1\sin(4\pi x))e^{-t}$. The observation point is $x_0 = 0.945 + \sqrt{2}/10{,}000$, and we take $N = 5$. Figure 2 shows the reconstructions for $\alpha = 1.2$ and $\alpha = 1.8$ under different noise levels. Table 2 presents the relative errors along with the values of μ at different noise levels for the two fractional orders.



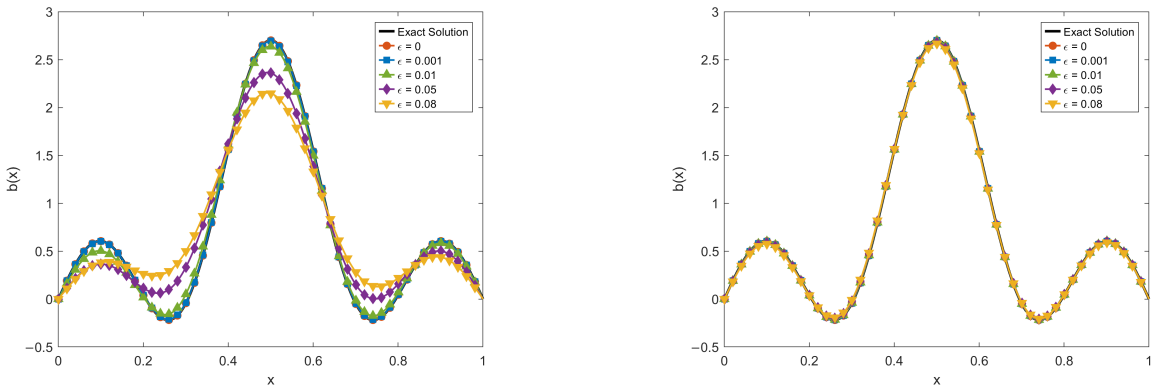
(a) $\alpha = 1.2$ **(b)** $\alpha = 1.8$

Figure 2. Numerical reconstructions for Example 2 under various noise levels with $\alpha = 1.2$ and $\alpha = 1.8$.

Table 2. Relative errors and μ under different noise levels for Example 2.

$e_r(\mu)$ ϵ / α	0	0.001	0.01	0.05	0.08
1.2	1.18e-08 (0)	5.79e-04 (9.16e-05)	5.79e-03 (2.89e-04)	2.89e-02 (6.36e-04)	4.63e-02 (7.97e-04)
1.8	1.99e-10 (0)	8.60e-05 (5.53e-04)	8.60e-04 (1.75e-03)	4.30e-03 (3.91e-03)	6.88e-03 (4.95e-03)

Example 3. Let the true initial velocity be $b(x) = 1.2\sin(\pi x) - 0.7\sin(3\pi x) + 0.8\sin(5\pi x)$, with $a(x) = 0.5\sin(\pi x)$ and $F(x,t) = 0.5\sin(\pi x)e^{-t}$. The observation point is $x_0 = 0.945 + \sqrt{2}/10{,}000$, and we take $N = 8$. Figure 3 shows the reconstructions for $\alpha = 1.2$ and $\alpha = 1.8$ under different noise levels. Table 3 presents the relative errors along with the values of μ at different noise levels for the two fractional orders.



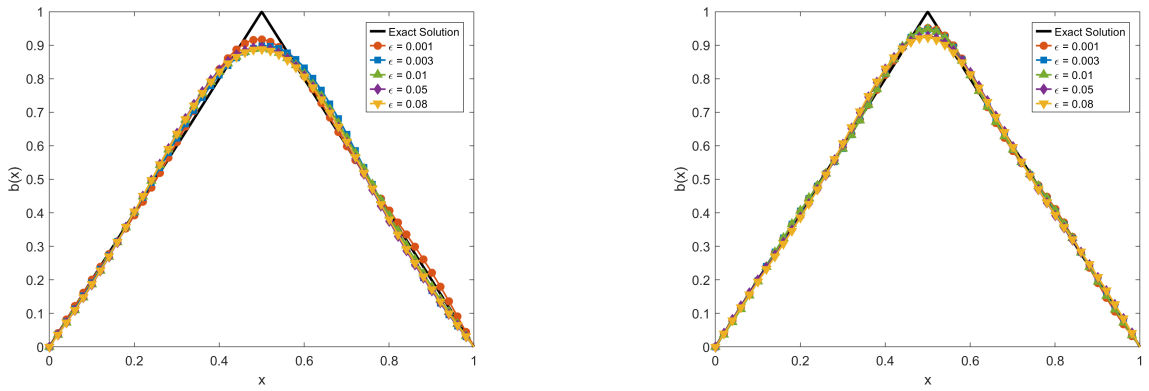
(a) $\alpha = 1.2$ **(b)** $\alpha = 1.8$

Figure 3. Numerical reconstructions for Example 3 under various noise levels with $\alpha = 1.2$ and $\alpha = 1.8$.

Table 3. Relative errors and μ under different noise levels for Example 3.

$e_r(\mu)$ ϵ / α	0	0.001	0.01	0.05	0.08
1.2	1.01e-07 (0)	3.28e-03 (5.13e-05)	4.81e-02 (1.49e-04)	1.79e-01 (3.70e-04)	2.67e-01 (4.99e-04)
1.8	5.52e-10 (0)	2.18e-04 (3.83e-04)	2.18e-03 (1.21e-03)	1.09e-02 (2.72e-03)	1.73e-02 (3.45e-03)

Example 4. Let the true initial velocity be $b(x) = 1 - |2x - 1|$, with $a(x) = 0.5\sin(2\pi x)$ and $F(x,t) = (0.3\sin(\pi x) + 0.1\sin(4\pi x))e^{-t}$. The observation point is $x_0 = 0.1 + \sqrt{2}/10{,}000$, and we take $N = 8$. Figure 4 shows the reconstructions for $\alpha = 1.2$ and $\alpha = 1.8$ under different noise levels. Table 4 presents the relative errors along with the values of μ at different noise levels for the two fractional orders.



(a) $\alpha = 1.2$ **(b)** $\alpha = 1.8$

Figure 4. Numerical reconstructions for Example 4 under various noise levels with $\alpha = 1.2$ and $\alpha = 1.8$.

Table 4. Relative errors and μ under different noise levels for Example 4.

$e_r(\mu)$ ϵ / α	0.001	0.003	0.01	0.05	0.08
1.2	3.33e-02 (3.78e-04)	5.03e-02 (4.05e-04)	4.93e-02 (1.40e-03)	5.12e-02 (3.06e-03)	5.11e-02 (3.72e-03)
1.8	1.87e-02 (9.99e-04)	1.77e-02 (2.87e-03)	1.78e-02 (5.06e-03)	2.85e-02 (6.65e-03)	3.03e-02 (1.04e-02)

Figures 1–4 compare the exact initial velocity $b(x)$ with the Gaussian-filtered reconstructions $b^{\mu,\delta}(x)$ for $\alpha = 1.2$ and $\alpha = 1.8$. For noise-free and low-noise data, the reconstructions agree closely with the exact profiles in the smooth examples. As the noise level increases, the errors generally increase, with a stronger deterioration for Example 3 when $\alpha = 1.2$. Example 4 also retains a visible truncation/regularization error even for low-noise data. Thus, Tables 1–4 should be interpreted as demonstrating noise-dependent stability within the tested discretizations rather than uniform accuracy over all examples and parameter choices.

For Table 5, Example 2 is used with $\alpha = 1.5$, $\epsilon = 0.01$, $\mu = 0.001$, $x_0 = 0.945 + \sqrt{2}/10{,}000$, $N_t = 2000$, and $N_x = 1000$. The exact initial velocity in this example contains only the first and third sine modes, so $N = 3$ already contains all active spatial modes of the exact solution. Increasing N introduces additional higher-frequency unknown coefficients. These directions are associated with weaker singular components of the discrete forward matrix and are therefore more susceptible to noise amplification. The error growth in Table 5 should consequently be viewed as a manifestation of the truncation–conditioning trade-off of the discrete inverse problem, not as evidence that increasing the spatial resolution is always beneficial or that the method is uniformly robust with respect to N.

For Table 6, Example 1 is tested with $\alpha = 1.6$, $\epsilon = 0.01$, $\mu = 0.001$, $M = 64$, $N_{\max} = 4$, and $x_0 = 0.085 + \sqrt{2}/10{,}000$. The reported errors remain of the same order under the tested grid refinements, indicating limited sensitivity to the chosen forward-grid resolution in this range. Table 7, obtained for the same example with $\alpha = 1.5$, illustrates the expected bias–stability trade-off with respect to μ: Overly large values oversmooth the reconstruction, whereas excessively small values may insufficiently suppress unstable singular components.

Table 5. Relative errors for Example 2 under different M and N.

e_r	$N = 3$	$N = 4$	$N = 5$	$N = 6$	$N = 7$
$M = 16$	0.00518	0.04938	0.09572	0.09680	0.10674
$M = 32$	0.00516	0.04912	0.09207	0.10460	0.10739
$M = 64$	0.00517	0.04902	0.09243	0.10479	0.10617
$M = 128$	0.00517	0.04902	0.09242	0.10479	0.10620

Table 6. Relative errors for Example 1 under different N_x and N_t.

e_r	$N_t = 1000$	$N_t = 1500$	$N_t = 2500$	$N_t = 3000$	$N_t = 3500$	$N_t = 4000$	$N_t = 4500$
$N_x = 500$	0.0043	0.0018	0.0011	0.0012	0.0014	0.0017	0.0020
$N_x = 1000$	0.0043	0.0018	0.0011	0.0012	0.0014	0.0017	0.0020

Table 7. Relative errors for Example 1 under different μ values.

μ	0.0001	0.0003	0.0010	0.0030	0.0100	0.0300	0.1000
e_r	0.0021	0.0021	0.0018	0.0029	0.0435	0.2849	0.7093

Tables 5–7 examine the influence of the truncation dimensions, the space–time grids, and the regularization parameter. In addition to the main reconstructions at $\alpha = 1.2$ and $\alpha = 1.8$, these parameter studies use the intermediate orders $\alpha = 1.5$ and $\alpha = 1.6$, providing supplementary checks away from the two endpoint test values.

Table 8. Relative errors for Example 2 at different interior observation points.

e_r \ x_0 / α	$0.085 + \sqrt{2}/10{,}000$	$0.1 + \sqrt{2}/10{,}000$	$0.3 + \sqrt{3}/10{,}000$	$0.6 + \sqrt{5}/10{,}000$	$0.85 + \sqrt{7}/10{,}000$
1.3	2.6972e-02	2.7392e-02	9.4900e-02	4.6458e-02	3.9500e-03
1.7	3.0570e-03	3.1169e-03	1.1276e-02	8.6361e-03	1.1137e-03

For Table 8, we fix $\epsilon = 0.01$ in Example 2 and vary only the interior observation point. For each observation point and for both $\alpha = 1.3$ and $\alpha = 1.7$, the parameter μ is determined independently by the discrete Morozov discrepancy principle with $\tau = 1.01$. The variation of the reported errors shows that even among observation points satisfying the uniqueness condition, the reconstruction accuracy can depend noticeably on the sensor location.

This dependence also has a conditioning interpretation: Because $\alpha_n(t) = tE_{\alpha,2}(-\lambda_n t^\alpha)\phi_n(x_0)$, the nth column of the discrete forward matrix contains the factor $\phi_n(x_0)$. Changing x_0 can therefore change the singular spectrum of the matrix; if $|\phi_n(x_0)|$ is small for a retained mode, the corresponding direction is weakly observable, which may reduce the smallest singular value and increase the condition number.

Thus, the uniqueness condition $\phi_n(x_0) \neq 0$ does not imply uniform numerical conditioning with respect to the observation point.

Table 9. Comparison of Gaussian spectral filtering and Tikhonov regularization for Example 2 with $\alpha = 1.5$.

Method	0	0.001	0.01	0.05	0.08	0.1
Gaussian spectral filtering	6.7248e-10	1.7059e-04	1.7060e-03	8.5292e-03	1.3646e-02	1.7056e-02
Tikhonov regularization	1.7052e-11	1.7059e-04	1.7054e-03	8.5145e-03	1.3608e-02	1.6997e-02

For the comparison in Table 9, we consider only $\alpha = 1.5$. The standard zero-order Tikhonov reconstruction is

$$\boldsymbol{c}_\mu^\delta = \arg\min_{\boldsymbol{c}} \left\{ \|A_{M,N}\boldsymbol{c} - \boldsymbol{H}_M^\delta\|_2^2 + \mu^2 \|\boldsymbol{c}\|_2^2 \right\}.$$

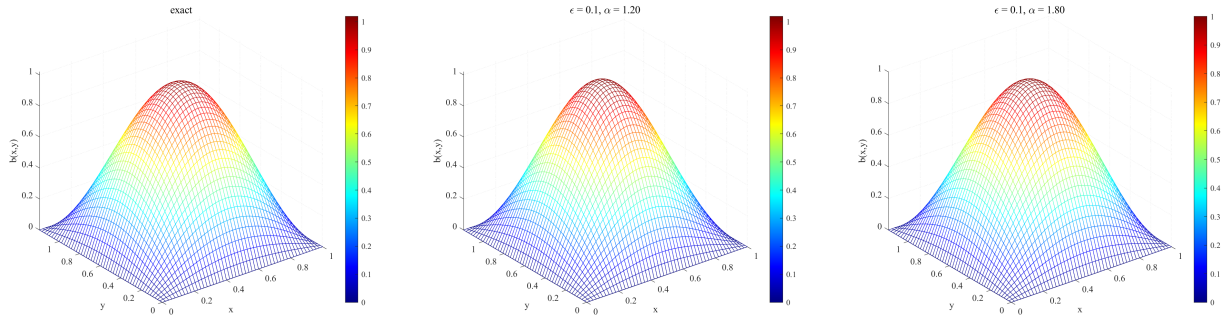
For both the Gaussian spectral filter and Tikhonov regularization, the regularization parameter is selected independently from the same noisy data by the discrete Morozov discrepancy principle with $\tau = 1.01$; the exact solution is used only to evaluate the relative reconstruction error. Under this common parameter-choice rule, the two methods give very similar errors over the tested noise levels.

5.2. Two-dimensional case

In the two-dimensional numerical examples, we take $M = 64$, $l_1 = 1$, $l_2 = 2^{1/4}$, $T = 1$, and $N_t = 2000$; the spatial evaluation grids use $N_x = N_y = 201$. The spatial truncation is chosen separately for the two examples: Example 5 uses $(N_1, N_2) = (2, 2)$, so $N = 4$, whereas Example 6 uses $(N_1, N_2) = (3, 1)$, so $N = 3$. These choices contain all nonzero modes of the corresponding exact initial velocities without introducing unnecessary additional modes. In both examples, μ is determined by the discrete Morozov discrepancy principle with $\tau = 1.01$. Moreover, $l_1^2/l_2^2 = 1/\sqrt{2} \notin \mathbb{Q}$, and the normalized coordinates of the observation points below are irrational, so the geometric assumptions of Corollary 2.5 are satisfied.

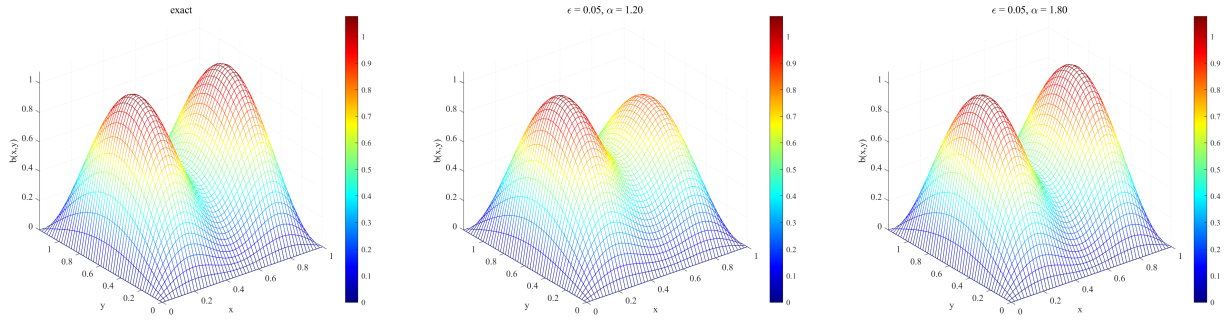
Example 5. Let the true initial velocity be $b(x, y) = \sin(\pi x)\sin\left(\pi y/2^{1/4}\right)$. Take $a(x, y) = 0.2\sin(\pi x)\sin\left(\pi y/2^{1/4}\right)$, $F(x, y, t) = 0.1e^{-t}\sin(\pi x)\sin\left(\pi y/2^{1/4}\right)$, and $x_0 = (x_0^1, x_0^2) = \left(\sqrt{2}/5,\ \sqrt{3}\,2^{1/4}/5\right)$. For this example, we use $(N_1, N_2) = (2, 2)$. Figure 5 shows the exact and reconstructed profiles for $\alpha = 1.2$ and $\alpha = 1.8$ at $\epsilon = 0.1$, and Table 10 reports the relative errors and the Morozov-selected values of μ under different noise levels.

Example 6. Let the true initial velocity be $b(x, y) = (\sin(\pi x) + 0.5\sin(3\pi x))\sin\left(\pi y/2^{1/4}\right)$. Take $a(x, y) = 0.2\sin(\pi x)\sin\left(\pi y/2^{1/4}\right)$, $F(x, y, t) = 0.1e^{-t}\sin(\pi x)\sin\left(\pi y/2^{1/4}\right)$, and $x_0 = (x_0^1, x_0^2) = \left(\sqrt{2}/10,\ \sqrt{3}\,2^{1/4}/10\right)$. For this example, we use $(N_1, N_2) = (3, 1)$. Figure 6 shows the exact and reconstructed profiles for $\alpha = 1.2$ and $\alpha = 1.8$ at $\epsilon = 0.05$, and Table 11 reports the relative errors and the Morozov-selected values of μ under different noise levels.



(a) Exact solution. **(b)** $\alpha = 1.2$. **(c)** $\alpha = 1.8$.

Figure 5. Exact and numerical solutions for Example 5.



(a) Exact solution. **(b)** $\alpha = 1.2$. **(c)** $\alpha = 1.8$.

Figure 6. Exact and numerical solutions for Example 6.

Table 10. Relative errors and μ under different noise levels for Example 5.

$e_r(\mu)$ ϵ / α	10^{-5}	0.001	0.01	0.05	0.1
1.2	1.36e-04 (3.03e-05)	1.34e-02 (3.08e-04)	4.42e-02 (1.32e-03)	1.00e-01 (3.51e-03)	1.04e-01 (4.92e-03)
1.8	8.54e-06 (1.56e-04)	8.52e-04 (1.56e-03)	8.33e-03 (5.02e-03)	3.64e-02 (1.21e-02)	5.75e-02 (1.83e-02)

Table 11. Relative errors and μ under different noise levels for Example 6.

$e_r(\mu)$ ϵ / α	10^{-5}	0.001	0.01	0.05	0.1
1.2	2.84e-05 (9.46e-06)	2.84e-03 (9.48e-05)	2.84e-02 (3.05e-04)	1.42e-01 (7.51e-04)	2.80e-01 (1.25e-03)
1.8	1.09e-06 (6.14e-05)	1.09e-04 (6.14e-04)	1.09e-03 (1.94e-03)	5.43e-03 (4.35e-03)	1.09e-02 (6.16e-03)

Figures 5 and 6 and Tables 10 and 11 show stable two-dimensional reconstructions over the tested noise range, with the expected deterioration as the noise level increases. Example 5 contains only the

lowest active spatial mode, whereas Example 6 also contains the higher x-mode $(3, 1)$ and becomes more sensitive to larger noise levels, especially for $\alpha = 1.2$. For both examples, the reconstructions with $\alpha = 1.8$ are more accurate than those with $\alpha = 1.2$ at the same noise level. These results illustrate that the reconstruction accuracy depends not only on the noise level but also on the fractional order and the spatial complexity of the target initial velocity.

6. Conclusions

This paper investigates the inverse initial-velocity problem for a time-fractional diffusion–wave equation in one- and two-dimensional settings, using measurements collected at a single interior point. To address the inherent ill-posedness, a Gaussian-type spectral filtering regularization scheme is introduced to damp unstable components associated with small singular values. Both a priori and Morozov-type a posteriori parameter-choice rules are analyzed, together with corresponding convergence error estimates. The numerical experiments support the feasibility of the method under noisy data and illustrate the dependence of the reconstruction accuracy on the observation location, truncation level, fractional order, and spatial complexity of the target.

Use of AI tools declaration

The authors declare they have not used Artificial Intelligence (AI) tools in the creation of this article.

Acknowledgments

This work was supported by the Natural Science Foundation of Xinjiang Uygur Autonomous Region (No. 2022D01C408).

Conflict of interest

The authors declare there are no conflicts of interest.

References

1. R. Metzler, J. Klafter, Subdiffusive transport close to thermal equilibrium: from the Langevin equation to fractional diffusion, *Phys. Rev. E*, **61** (2000), 6308–6311. https://doi.org/10.1103/PhysRevE.61.6308
2. S. B. Yuste, L. Acedo, K. Lindenberg, Reaction front in an $A + B \to C$ reaction-subdiffusion process, *Phys. Rev. E*, **69** (2004), 036126. https://doi.org/10.1103/PhysRevE.69.036126
3. I. M. Sokolov, J. Klafter, From diffusion to anomalous diffusion: a century after Einstein's Brownian motion, *Chaos*, **15** (2005), 026103. https://doi.org/10.1063/1.1860472
4. H. W. Engl, M. Hanke, A. Neubauer, *Regularization of Inverse Problems*, Kluwer Academic Publishers, Dordrecht, 1996.
5. A. Kirsch, *An Introduction to the Mathematical Theory of Inverse Problems*, Springer-Verlag, New York, 2021. https://doi.org/10.1007/978-3-030-63343-1

6. T. Wei, Y. Zhang, The backward problem for a time-fractional diffusion-wave equation in a bounded domain, *Comput. Math. Appl.*, **75** (2018), 3632–3648. https://doi.org/10.1016/j.camwa.2018.02.022
7. G. Floridia, M. Yamamoto, Backward problems in time for fractional diffusion-wave equation, *Inverse Probl.*, **36** (2020), 125016. https://doi.org/10.1088/1361-6420/abbc5e
8. C. Shi, H. Cheng, W. Fan, An iterative generalized quasi-boundary value regularization method for the backward problem of time fractional diffusion wave equation in a cylinder, *Numerical Algorithms*, **94** (2023), 1619–1651. https://doi.org/10.1007/s11075-023-01549-2
9. J. Wen, Y. P. Wang, The quasi-reversibility regularization method for backward problems of the time-fractional diffusion-wave equation, *Phys. Scr.*, **98** (2023), 095250. https://doi.org/10.1088/1402-4896/acf0f8
10. F. Yang, Y. Zhang, X. X. Li, Landweber iterative method for identifying the initial value problem of the time-space fractional diffusion-wave equation, *Numerical Algorithms*, **83** (2020), 1509–1530. https://doi.org/10.1007/s11075-019-00734-6
11. T. Wei, K. F. Liao, Identifying a time-dependent zeroth-order coefficient in a time-fractional diffusion-wave equation by using the measured data at a boundary point, *Appl. Anal.*, **101** (2022), 6522–6547. https://doi.org/10.1080/00036811.2021.1932834
12. T. Wei, J. Xian, Determining a time-dependent coefficient in a time-fractional diffusion-wave equation with the Caputo derivative by an additional integral condition, *J. Comput. Appl. Math.*, **404** (2022), 113910. https://doi.org/10.1016/j.cam.2021.113910
13. Y. Kian, Z. Y. Li, Y. K. Liu, M. Yamamoto, The uniqueness of inverse problems for a fractional equation with a single measurement, *Math. Ann.*, **380** (2021), 1465–1495. https://doi.org/10.1007/s00208-020-02027-z
14. C. Shi, H. Cheng, Identify the Robin coefficient in an inhomogeneous time-fractional diffusion-wave equation, *J. Comput. Appl. Math.*, **434** (2023), 115337. https://doi.org/10.1016/j.cam.2023.115337
15. D. K. Durdiev, H. H. Turdiev, Inverse coefficient problem for a time-fractional wave equation with initial-boundary and integral type overdetermination conditions, *Math. Methods Appl. Sci.*, **47** (2024), 5329–5340. https://doi.org/10.1002/mma.9867
16. E. Bazhlekova, Application of subordination principle to coefficient inverse problem for multi-term time-fractional wave equation, *Fract. Calc. Appl. Anal.*, **27** (2024), 1596–1610. https://doi.org/10.1007/s13540-024-00284-2
17. T. Wei, R. Deng, Simultaneous determination of the order and a coefficient in a fractional diffusion-wave equation, *J. Sci. Comput.*, **103** (2025), 31. https://doi.org/10.1007/s10915-025-02836-x
18. X. H. Jing, M. Yamamoto, Simultaneous uniqueness for multiple parameters identification in a fractional diffusion-wave equation, *Inverse Probl. Imaging*, **16** (2022), 1199–1217. https://doi.org/10.3934/ipi.2022019
19. Y. H. Luo, M. J. Pei, T. Wei, Simultaneous identification of the order and potential coefficient in a time fractional diffusion-wave equation by a deep neural networks method, *Comput. Appl. Math.*, **44** (2025), 332. https://doi.org/10.1007/s40314-025-03295-8

20. M. Yamamoto, Uniqueness in determining fractional orders of derivatives and initial values, *Inverse Probl.*, **37** (2021), 095006. https://doi.org/10.1088/1361-6420/abf9e9

21. M. Yamamoto, Uniqueness for inverse source problems for fractional diffusion-wave equations by data during not acting time, *Inverse Probl.*, **39** (2023), 024004. https://doi.org/10.1088/1361-6420/aca55c

22. K. Sakamoto, M. Yamamoto, Initial value/boundary value problems for fractional diffusion-wave equations and applications to some inverse problems, *J. Math. Anal. Appl.*, **382** (2011), 426–447. https://doi.org/10.1016/j.jmaa.2011.04.058

23. X. C. Huang, M. Yamamoto, Well-posedness of initial-boundary value problem for time-fractional diffusion/wave equation with time-dependent coefficients, *J. Evol. Equations*, **25** (2025), 68. https://doi.org/10.1007/s00028-025-01094-6

24. R. Gorenflo, Y. Luchko, M. Yamamoto, Time-fractional diffusion equation in the fractional Sobolev spaces, *Fract. Calc. Appl. Anal.*, **18** (2015), 799–820. https://doi.org/10.1515/fca-2015-0048

25. Z. Z. Sun, X. N. Wu, A fully discrete difference scheme for a diffusion-wave system, *Appl. Numer. Math.*, **56** (2006), 193–209. https://doi.org/10.1016/j.apnum.2005.03.003

26. H. Jiang, F. Liu, I. Turner, K. Burrage, Analytical solutions for the multi-term time-fractional diffusion-wave/diffusion equations in a finite domain, *Comput. Math. Appl.*, **64** (2012), 3377–3388. https://doi.org/10.1016/j.camwa.2012.02.042

27. B. T. Jin, R. Lazarov, Z. Zhou, Two fully discrete schemes for fractional diffusion and diffusion-wave equations with nonsmooth data, *SIAM J. Sci. Comput.*, **38** (2016), A146–A170. https://doi.org/10.1137/140979563

28. C. P. Li, F. H. Zeng, Finite difference methods for fractional differential equations, *Int. J. Bifurcation Chaos*, **22** (2012), 1230014. https://doi.org/10.1142/S0218127412300145

29. A. A. Kilbas, H. M. Srivastava, J. J. Trujillo, *Theory and Applications of Fractional Differential Equations*, North-Holland Mathematics Studies, Elsevier, Amsterdam, 2006. https://doi.org/10.1016/S0304-0208(06)X8001-5

30. I. Podlubny, *Fractional Differential Equations: An Introduction to Fractional Derivatives, Fractional Differential Equations, to Methods of Their Solution and Some of Their Applications*, Mathematics in Science and Engineering, Academic Press, San Diego, 1999. https://doi.org/10.1016/S0076-5392(99)X8001-5

31. D. A. Murio, The mollification method and the numerical solution of an inverse heat conduction problem, *SIAM J. Sci. Stat. Comput.*, **2** (1981), 17–34. https://doi.org/10.1137/0902003

32. P. C. Hansen, *Rank-Deficient and Discrete Ill-Posed Problems: Numerical Aspects of Linear Inversion*, SIAM, Philadelphia, 1998. https://doi.org/10.1137/1.9780898719697

33. D. A. Murio, *The Mollification Method and the Numerical Solution of Ill-Posed Problems*, John Wiley & Sons, New York, 1993. https://doi.org/10.1002/9781118033210

34. F. Berntsson, A spectral method for solving the sideways heat equation, *Inverse Probl.*, **15** (1999), 891–906. https://doi.org/10.1088/0266-5611/15/4/305

35. F. Bozzoli, L. Cattani, A. Mocerino, S. Rainieri, F. S. V. Bazán, A novel method for estimating the distribution of convective heat flux in ducts: Gaussian filtered singular value decomposition, *Inverse Probl. Sci. Eng.*, **27** (2019), 1595–1607. https://doi.org/10.1080/17415977.2018.1540615

36. V. A. Morozov, *Methods for Solving Incorrectly Posed Problems*, Springer, New York, 1984. https://doi.org/10.1007/978-1-4612-5280-1

37. J. G. Wang, T. Wei, Y. B. Zhou, Tikhonov regularization method for a backward problem for the time-fractional diffusion equation, *Appl. Math. Modell.*, **37** (2013), 8518–8532. https://doi.org/10.1016/j.apm.2013.03.071



AIMS Press

© 2027 the Author(s), licensee AIMS Press. This is an open access article distributed under the terms of the Creative Commons Attribution License (https://creativecommons.org/licenses/by/4.0)